ELSEVIER

Ocean Modelling 4 (2002) 89–120

Ocean Modelling

www.elsevier.com/locate/omodol

Evaluation of ocean model ventilation with CFC-11: comparison of 13 global ocean models

J.-C. Dutay [a,*], J.L. Bullister [b], S.C. Doney [c], J.C. Orr [a], R. Najjar [d], K. Caldeira [e], J.-M. Campin [f], H. Drange [g], M. Follows [h], Y. Gao [g], N. Gruber [i], M.W. Hecht [c], A. Ishida [j], F. Joos [k], K. Lindsay [c], G. Madec [l], E. Maier-Reimer [m], J.C. Marshall [h], R.J. Matear [n], P. Monfray [a], A. Mouchet [q], G.-K. Plattner [k], J. Sarmiento [i], R. Schlitzer [o], R. Slater [i], I.J. Totterdell [p], M.-F. Weirig [o], Y. Yamanaka [j], A. Yool [p]

[a] *Laboratoire des Sciences du Climat et de l'Environnement, Gif sur Yvette, France*
[b] *Pacific Marine Environmental Laboratory, NOAA, Seattle, WA, USA*
[c] *National Center for Atmospheric Research, Boulder, CO, USA*
[d] *Pensylvania State University, Pensylvania, USA*
[e] *Lawrence Livermore National Laboratory, Livermore, CA, USA*
[f] *Institut d'Astronomie et de Geophysique G. Lemaitre, University Catholique de Louvain, Belgium*
[g] *Nansen Enviromental and Remote Sensing Center, Norway*
[h] *Massachussets Institute of Technology, Cambridge, MA, USA*
[i] *Atmospheric and Oceanic Sciences Program, Princeton University, Princeton, NJ, USA*
[j] *Institute for Global Change Research, Tokyo, Japan*
[k] *Physics Institute Univeristy of Bern, Switzerland*
[l] *Laboratoire d'Océanographie Dynamique et de Climatologie Paris, France*
[m] *Max Planck Institut fuer Meteorologie, Hamburg, Germany*
[n] *Commonwealth Science and Industrial Research Organization, Hobart, Australia*
[o] *Alfred Wegener Institute for Polar and Marine Research, Bremerhaven, Germany*
[p] *Southampton Oceanography Centre, Southampton, UK*
[q] *Astrophysics et Geophysics Institute, University of Liege, Belgium*

Received 25 September 2000; received in revised form 30 July 2001; accepted 30 July 2001

Abstract

We compared the 13 models participating in the Ocean Carbon Model Intercomparison Project (OCMIP) with regards to their skill in matching observed distributions of CFC-11. This analysis characterizes the abilities of these models to ventilate the ocean on timescales relevant for anthropogenic CO_2

* Corresponding author. Tel.: +33-1-6908-3112; fax: +33-1-6908-7716.
E-mail address: dutay@lsce.saclay.cea.fr (J.-C. Dutay).

1463-5003/02/$ - see front matter
PII: S1463-5003(01)00013-0

uptake. We found a large range in the modeled global inventory (±30%), mainly due to differences in ventilation from the high latitudes. In the Southern Ocean, models differ particularly in the longitudinal distribution of the CFC uptake in the intermediate water, whereas the latitudinal distribution is mainly controlled by the subgrid-scale parameterization. Models with isopycnal diffusion and eddy-induced velocity parameterization produce more realistic intermediate water ventilation. Deep and bottom water ventilation also varies substantially between the models. Models coupled to a sea-ice model systematically provide more realistic AABW formation source region; however these same models also largely overestimate AABW ventilation if no specific parameterization of brine rejection during sea-ice formation is included. In the North Pacific Ocean, all models exhibit a systematic large underestimation of the CFC uptake in the thermocline of the subtropical gyre, while no systematic difference toward the observations is found in the subpolar gyre. In the North Atlantic Ocean, the CFC uptake is globally underestimated in subsurface. In the deep ocean, all but the adjoint model, failed to produce the two recently ventilated branches observed in the North Atlantic Deep Water (NADW). Furthermore, simulated transport in the Deep Western Boundary Current (DWBC) is too sluggish in all but the isopycnal model, where it is too rapid.

Keywords: Models; Ocean ventilation; Transient tracers; CFC

1. Introduction

Ocean carbon models offer a means to study and improve our understanding of the carbon cycle in the ocean and its feedback on the climate system. Due to the importance of CO_2 to the greenhouse effect, many research groups have developed ocean carbon models in order to better understand the role of oceanic CO_2 uptake on past, present and future atmospheric CO_2 concentrations. The Ocean Carbon-cycle Model Intercomparison Project (OCMIP) is part of this effort. It was initiated because models improve more rapidly when resources are pooled and understanding is shared among modelling groups, and when they are systematically evaluated against observations (Orr, 1999). Simulations with the four models that participated in the first phase of OCMIP, all suggest that the Southern Ocean is a region of large uptake of anthropogenic CO_2, with the models giving widely different views of the regional distribution of this uptake (Orr et al., 2001). Evaluation of the performance of these models is based on their comparison with data-based estimates for anthropogenic CO_2 (Gruber et al., 1996; Sabine et al., 1999) and bomb C-14 (Broecker et al., 1995). However, these data-based estimates may be subject to large systematic errors in some regions such as the Southern Ocean. Thus ocean carbon cycle models require further independent evaluation with other geochemical tracers, whose oceanic distribution and uptake are better known.

In the second phase of OCMIP, the number of models has increased from 4 to 13 (Table 1). OCMIP-2 also includes evaluation of the models' circulation fields with some new tracers, including chlorofluorocarbons (CFCs). CFC-11 and CFC-12 are gases of purely anthropogenic origin, whose atmospheric concentrations have increased from zero since the 1930s. CFC-11 and CFC-12 enter the surface ocean via gas exchange and are carried within the ocean as passive and conservative tracers of circulation and mixing processes that occur on decadal timescales (Bullister and Weiss, 1983; Weiss et al., 1985; Wallace and Lazier, 1988; Warner and Weiss, 1992; Doney and Bullister, 1992; Smethie, 1993; Roether et al., 1993; Rhein, 1994; Warner et al., 1996;

Table 1
List of OCMIP-2 groups

Modeling groups
AWI (Alfred Wegener Institute for Polar and Marine Research), Bremerhaven, Germany
CSIRO (Commonwealth Science and Industrial Research Organization), Hobart, Australia
IGCR/CCSR (Institute for Global Change Research), Tokyo, Japan
IPSL (Institut Pierre Simon Laplace), Paris, France
LLNL (Lawrence Livermore National Laboratory), Livermore, CA, USA
MIT (Massachussets Institute of Technology), Cambridge, MA, USA
MPIM (Max Planck Institut fuer Meteorologie), Hamburg, Germany
NCAR (National Center for Atmospheric Research), Boulder, CO, USA
NERSC (Nansen Enviromental and Remote Sensing Center), Norway
PIUB (Physics Institute, Univeristy of Bern), Switzerland
PRINCEton (Princeton University AOS, OTL/GFDL), Princeton, NJ, USA
SOC (Southampton Oceanography Centre)/SUDO/Hadley center (UK Met. Office), England
UL (University of Liege)/UCL (Université Catholique de Louvain), Belgium
Data groups
PMEL (Pacific Marine Environmental Laboratory), NOAA, Seattle, WA, USA
PSU (Pennsylvania State University), PA, USA
PRINCEton (Princeton University AOS, OTL/GFDL), Princeton, NJ, USA

Smythe-Wright and Boswell, 1998; Andrié et al., 1999). Thus, CFCs are qualitatively similar to anthropogenic CO_2, and this has motivated a number of investigators to use CFCs to evaluate the ability of ocean circulation models to simulate the uptake and redistribution of anthropogenic CO_2 in the oceans (England, 1995; Robitaille and Weaver, 1995; England and Hirst, 1997; Heinze et al., 1998; Dutay, 1998; Haine and Gray, 1999). The transfer of CFC-11 and CFC-12 in the ocean is well known, and their oceanic concentrations are measured with high precision. Measurements are available globally, with greatly extended coverage from the recent World Ocean Circulation Experiment (WOCE). Along the sections, the temporal and spatial resolution of the CFC data is ''very high'', but in the ocean as a whole the resolution is ''very low'', even for WOCE.

In this paper we have compared and evaluated standard CFC-11 simulations from the 13 models participating in OCMIP-2. Our analysis focused on the middle and high latitude ocean ventilation, where most of the anthropogenic CO_2 is absorbed in the ocean. This paper has two main goals. First, we wish to characterize the abilities of the models to ventilate the ocean on the timescales relevant for anthropogenic CO_2 uptake. This characterization is necessary for assessing the accuracy of the predictions of anthropogenic CO_2 uptake by the OCMIP-2 models. The second goal of the paper is to present to the ocean and climate modeling communities an evaluation of the decadal scale ventilation characteristics of the major state-of-the-art Ocean General Circulation Models (OGCMs) used in long-term climate modeling today. Our evaluation is largely qualitative in that we cannot pin down the exact causes for differences among the models and between the models and observations. However, we are hopeful that our effort will set standards and motivate individual modeling groups to develop new parameterizations and conduct sensitivity studies that will ultimately improve coarse-resolution OGCMs.

Below, we begin by providing a brief description of model characteristics and the OCMIP simulations for CFC-11. We show only the CFC-11 results; because the CFC-12 results lead to the same conclusions. Then we present results, first as integrative diagnostics in order to capture the broad characteristics and differences among models, to compare their time evolution and the spatial distribution of CFC-11 uptake. Subsequently, we compare models results along observed sections and on specific water mass surfaces in order to evaluate the behavior of the models in the regions that models indicate are quantitatively important for anthropogenic CO_2 uptake. Finally, we attempt to isolate the features that appear to be similar among some models and try to relate them, where possible, to model forcing or physics.

2. Description of the circulation models

The general characteristics of the 13 models participating in OCMIP-2 are presented in Table 2. All 13 models have global coverage, with coarse, non-eddy resolving horizontal resolution; however, three of the models (IGCR, MIT and NERSC) lack an Arctic Ocean. All but three of the models are primitive equation models (Bryan, 1969). The exceptions are MPIM, which neglects non-linear terms in the advection equation (Large-scale Geostrophic Model) (Maier-Reimer, 1993), AWI, which uses an adjoint technique to derive the circulation from hydrographic and geochemical data (temperature, salinity, alkalinity, phosphate, dissolved inorganic carbon, oxygen, silicate and nitrate) (Schlitzer, 1999), and PIUB where momentum equations are balances between coriolis forces, horizontal pressure gradients and zonal wind stress (Stocker et al., 1992). The PIUB model is also a zonally averaged basin model. One model uses an isopycnal vertical coordinate (NERSC). The dynamical forcing (heat flux, fresh water flux and wind stress) is different in each model. Three of the models, AWI, IGCR and PIUB, use annually averaged forcing. Three models, LLNL, MPIM, UL are coupled to sea-ice models that include both thermodynamics and sea-ice dynamics. The PIUB model is coupled with a thermodynamic sea-ice model and an energy balance model of the atmosphere.

Parameterization of ocean physics also differs among the models. Models differ in their subgrid scale parameterization, which has a large effect on the predicted circulation. The lateral subgrid-scale mixing is horizontal in three models (IGCR, MPIM and UL), while the other models orient such mixing along isopycnal surfaces. Most of the latter use the eddy-induced velocity parameterization proposed by Gent et al. (1995) (hereafter GM). Most of the models have a prescribed profile of the vertical eddy diffusion coefficient, but some have a more sophisticated parameterization, such as the Kraus and Turner (1967) mixed layer scheme (SOC), the non-local K-profile parameterization (KPP) of the boundary layer from Large et al. (1994) (NCAR), or a turbulent kinetic energy (TKE) closure parameterization in the IPSL, UL and NERSC models (Gaspar et al., 1990; Goosse et al., 1999). The IPSL model applies a subsurface restoring to climatological temperature and salinity in the ocean interior below the mixed layer. This "robust diagnostic" forcing is reduced in the vicinity of land and in the polar region and suppressed at the equator (Madec et al., 1998). Bottom topography in the models differs considerably, which affects bottom water flow pathways. Other factors, such as the vertical discretization, the advection scheme and bottom boundary layer schemes also differ, which may affect the thermohaline circulation in this class of models. Further details of each model are provided in the references cited in Table 2.

Table 2
Model characteristics

	AWI	CSIRO	IGCR	IPSL	LLNL	MIT	MPLM	NERSC	NCAR	PIUB	PRIN	SOC	UL
Horizontal resolution (lon × lat)	5° × 4°–2.5° × 2°	5.6° × 3.2°	4° × 4°	From 2° × 1.5° to 0.5° Eq.	4° × 2°	2.8° × 2.8°	5° × 5°	2° × 3.2° cos(lat)	3.6° × 1.8°–0.8°	Zonally basin average	3.75° × 4.5°	2.5° × 3.75°	3° × 3°
Seasonality	No	Yes	No	Yes	Yes	Yes	Yes	Yes	Yes	No	Yes	Yes	Yes
Surface boundary conditions	Adjusted	T, S seasonal restoring	Levitus T, S annual restoring + N. All cooling	Flux + restoring	Bulk formula	Flux + restoring	Restoring	Bulk formula	Bulk formula	Coupled to EBM of atmosphere	Restoring AMIP SST Levitus SSS + flux	Restoring + flux	Bulk formula
Lateral subgrid-scale mixing	ISOP	ISOP + GM	HOR	ISOP + GM	ISOP + GM	ISOP + GM	HOR	ISOP	ISOP + GM	HOR	ISOP + GM	ISOP + GM	HOR
Mixed layer	–	–	–	TKE		–		TKE	KPP		–	Kraus and Turner	TKE
Sea-ice model	–	–	–	–	Yes	–	Yes	–	S restoring	Brine rejection	–		Yes
Off line/online	Off	On	Off	Off	On	On	Off	On	On	On	On	On	On
Reference	Schlitzer (1999)	Matear and Hirst (1999)	Yamanaka and Tajika (1996)	Madec et al. (1998)	Duffy et al. (1997)	Marshall et al. (1997)	Maier-Reimer et al. (1993)	Bleck et al. (1992)	Doney and Hecht (in press)	Stocker et al. (1992)	Gnanadesikan et al. (in press)	Gordon et al. (2000)	Goosse and Fichefet (1999)

EBM: Energy Balance Model; AMIP: Atmospheric Model Intercomparaison Project; Levitus: Climatological atlas of the world ocean, NOAA, 1982; HOR, ISOP, GM: Horizontal, Isopycnal, Gent and Mc Williams parameterization; TKE: Turbulent Kinetic Energy closure; KPP: non-local boundary layer parameterization, Large et al. (1994).

3. Parameterization of the air–sea CFC flux

For OCMIP-2, passive tracer fluxes at the air–sea interface are calculated in a common way for all the models. For the CFC simulations, which span 1932–1997, the net downward flux (Q) is calculated according to the classical formulation of air–sea gas exchange:

$$Q = k\left(FP_{\mathrm{cfc}}\frac{P}{P_0} - C_{\mathrm{s}}\right), \tag{1}$$

where k is the air–sea gas transfer velocity, F is the CFC solubility function, P_{cfc} is the CFC atmospheric partial pressure in dry air at one atmosphere total pressure, P is the monthly total air pressure at sea level from Esbensen and Kushnir (1981), P_0 is 1 atm, and C_{s} is the modeled sea surface tracer concentration. More specifically, F is the CFC solubility function in seawater (Warner and Weiss, 1985) using modeled sea surface temperature (SST) and salinity (SSS). P_{cfc} is assumed to be uniform in each hemisphere poleward of 10° latitude (Fig. 1(a)), with temporal values from the reconstructed annual mean mole fraction of P_{cfc} at 41°S and 45°N (Walker et al., 2000). Between 10°S and 10°N, we made a linear transition between the two hemispheres.

The formulation of air–sea gas transfer velocity in units of cm/h is from Wanninkhof (1992):

$$k = k_0(1-R)(u^2 + \langle v\rangle)(Sc/660)^{-1/2}, \tag{2}$$

where R is sea-ice fraction, Sc is the Schmidt number of the gas and u and $\langle v\rangle$ are the monthly mean (m/s) and the variance (m^2/s^2) of instantaneous wind speed at 10 m, respectively. In our study, the sea-ice fraction is prescribed from the Walsh (1978) and Zwally et al. (1983) climatologies, wind speed information is taken from the first and second Special Sensor Microwave Imager (SSMI) satellite data prepared as described in Boutin and Etcheto (1997) and Orr et al. (2001). The Schmidt numbers of the CFCs are estimated from modeled SST with the formulation of Zheng et al. (1998). Finally, k_0 ($= 0.31$ cm s^2/h m^2) is a constant that has been calibrated so that our global mean K for CO_2 matches the Broecker et al. (1986) radiocarbon-calibrated estimate of 0.061 mol C/m^2 yr μatm.

4. Results

4.1. CFC inventories and fluxes

In each model, the global CFC-11 inventory (the global amount of this tracer absorbed by the oceans) follows the increase of the CFC-11 partial pressure in the atmosphere (Fig. 1). Simulated inventories exhibit a standard deviation of about 20% and a range of about ±30% around the mean. Extrema clearly stand out: the uptake of UL and NERSC are largest while that of PRINCE is lowest. The evolution of the inventory in each model is linearly related to that in all others (r^2 of at least 0.99) (Fig. 1(c)).

With similar temporal evolution, one might also expect similar spatial structure. The CFC-11 cumulative flux distribution at the air–sea interface (Fig. 2), which is the time-integrated flux of the tracer into the ocean since the beginning of the simulations (1932), provides a signature of modeled water mass ventilation and transformation (e.g. upwelling). Uptake is consistently high

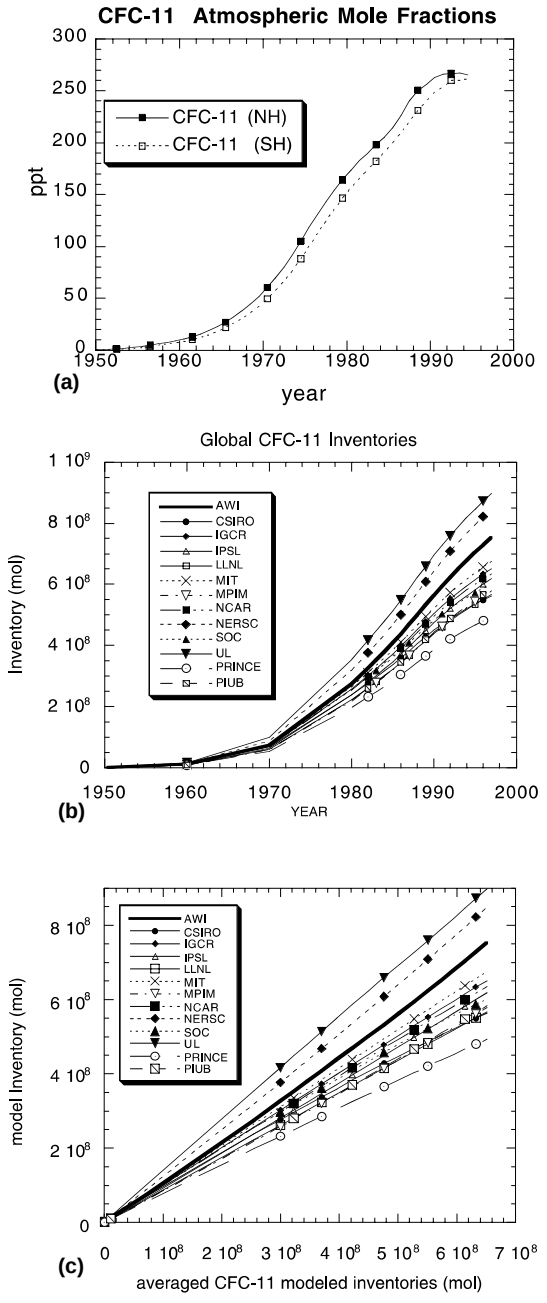

Fig. 1. Temporal evolution of (a) the CFC-11 atmospheric mole fraction in both hemispheres and (b) simulated global CFC-11 inventory. (c) Global CFC-11 model inventory as a function of the average global CFC-11 inventory of all the models.

mainly in regions of cold winter SST and strong vertical mixing such as the Southern Ocean, the North Atlantic Ocean and the Northwestern Pacific Ocean. Uptake is also high in the Equatorial Pacific due to upwelling of subsurface waters that are impoverished in CFC. Uptake is two orders

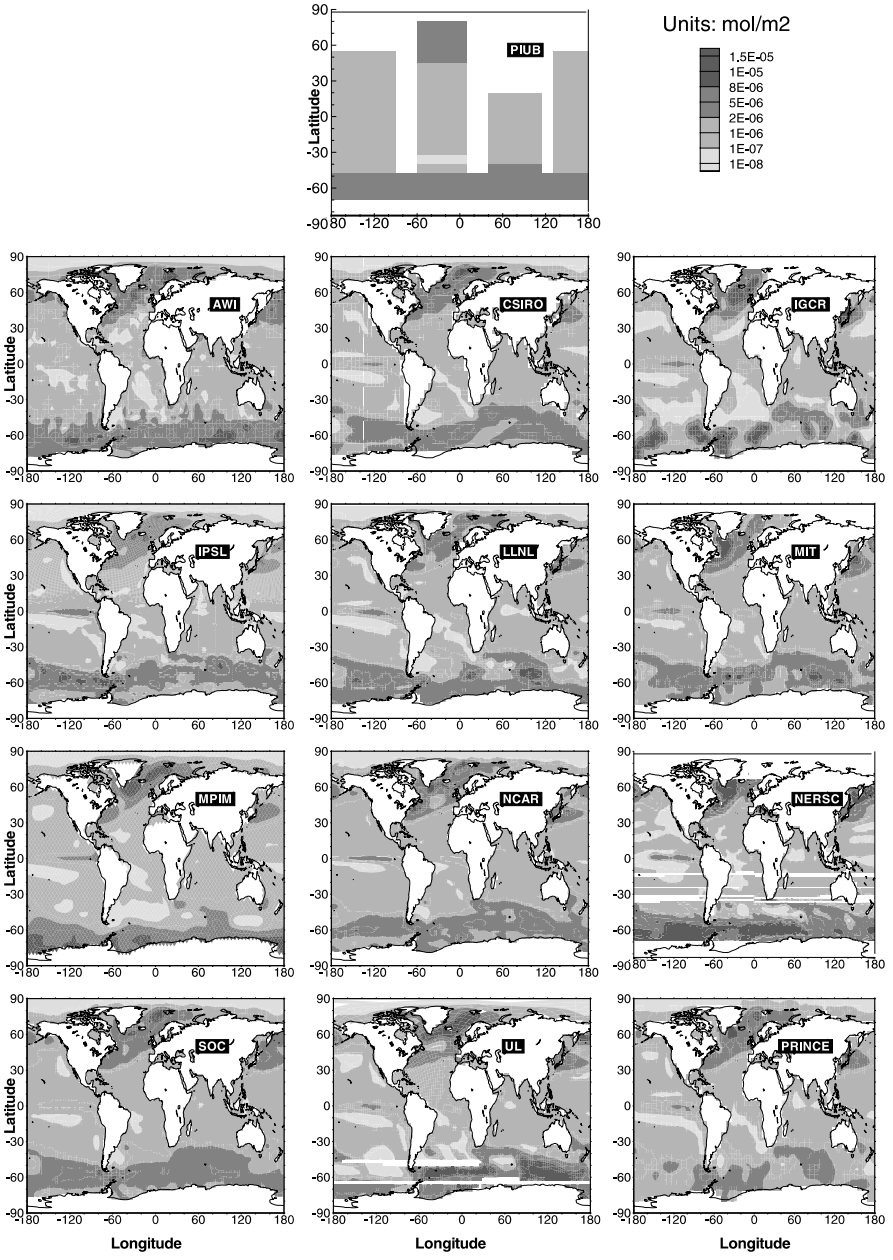

Fig. 2. Models' cumulative CFC11 flux in 1989. Units: mol/m^2.

of magnitude lower in the subtropics. Despite such similarities in the large-scale pattern of uptake, the detailed spatial structure differs substantially among models. Simulated CFC-11 uptake differs by up to an order of magnitude, especially in the Southern Ocean, where the greatest proportion of CFC-11 is absorbed in all the models. For instance, two models (IPSL and SOC) exhibit maximum uptake in the South Pacific and South Indian Oceans, whereas three other models

(CSIRO, UL and PRINCE) absorb most in the South Atlantic and South Indian Oceans, and the remaining models spread uptake throughout all three sectors of the Southern Ocean (Fig. 2). The MPIM and NERSC stand apart in that maximum uptake occurs adjacent to the Antarctic Coast; in the other models, most uptake is located offshore in the Antarctic Circumpolar Current (ACC). All models show similar dominance of the southern hemisphere with regard to CFC-11 uptake, from 60% (MPI and PRINCE) to 70% (UL and NERSC) of the total (Table 3).

4.2. North Pacific

In the North Pacific Ocean, all the models have their highest CFC-11 uptake near the Kuroshio extension just north of 30°N (Fig. 2), where the North Pacific Subtropical Mode Water (NPSTW) is formed (Suga et al., 1997), and where the winter mixed layer is deepest in this basin (Qiu and Huang, 1995). Uptake is also large in the North Pacific subpolar gyre, just south-east of the Bering Strait in most of the models.

An opportunity to evaluate the simulated CFC-11 distribution in this region of the North Pacific is provided by the WOCE P13 section at 165°E (Sonnerup et al., 1999). This section is plotted in Fig. 3 along with the corresponding section in each models. This figure, and others like it that show observed and modeled CFC sections, depict the model results for the same month and year that the measurements were made. Ventilation in both the observation and models is restricted to the thermocline in the North Pacific. Below 2000 m, CFC-11 concentrations are negligible, testifying to the lack of deep water formation. The only exception is the UL model, which shows an unrealistic penetration of CFC-11 to the bottom near the Bering strait.

To more quantitatively evaluate the CFC uptake, we define the local inventory of CFC-11 and CFC-11 partial pressure (PCFC-11) as their vertical integral (mol/m^2; 10^{-9} atm m) and the penetration depth (m) as the vertical integral divided by the surface concentration. Vertical integrals in the observations are computed using a trapezoidal method, while those from the models use the full model resolution. PCFC-11 inventories enable to remove the effects of temperature biases in the models and assess how much of the differences are due to the circulation. The local inventory and penetration depth are presented in Fig. 4 for the WOCE P-13 section. In the observations, the greatest CFC-11 penetration depth is around 1100 m and occurs in the subtropical gyre between 20°N and 40°N (Fig. 4(c)), where the lower thermocline is ventilated by intermediate water formed in the Sea of Okhotsk (Warner et al., 1996). The penetration depth is shallower (200–300 m) in the subpolar gyre where large stratification due to the vertical salinity gradients prevents deep penetration of CFCs (Warren, 1983). Models exhibit their greatest penetration depths of CFC-11 in the subtropical gyre between 20°N and 40°N, but they do not exceed 900 m and thus are smaller than observed (Fig. 4(b)). Simulated CFC-11 and PCFC-11 inventories in this latitudinal band are systematically too low, being at least 30% smaller than the observed inventory. The magnitude of these inventories varies by 60% among the models. The simulated penetration depths and inventories do not always correspond due to differences in stratification among models. As a whole, the models do not have a systematic bias in the subpolar gyre, north of 40°N (Fig. 4(a)). About half the models (LLNL, IPSL, MPIM, PIUB, PRINCE) underestimate that regions observed CFC-11 inventory; the others overestimate it, with some (UL, NERSC, NCAR, MIT) estimating values that are twice as large as those observed.

Table 3
Global and hemispheric CFC-11 uptake in 1989, units: 10^{18} mol. ratio of Northern Hemisphere CFC-11 uptake/Global CFC-11 uptake, units: percent

	AWI	CSIRO	IGCR	IPSL	LINL	MIT	MPIM	NCAR	NERSC	PIUB	PRINCE	SOC	UL
Global CFC-11 uptake	5.4	4.3	4.9	4.5	4.2	4.9	4.2	4.4	6.1	4.3	3.7	4.6	6.6
NH CFC-11 uptake	1.7	1.5	1.6	1.4	1.4	1.7	1.6	1.7	1.9	1.4	1.6	1.6	2.0
SH CFC-11 uptake	3.6	2.8	3.3	3.1	2.8	3.2	2.5	2.8	4.2	2.9	2.1	2.9	4.6
NH/global (%)	32.3	34.2	32.6	31.4	33.0	34.8	39.0	37.4	31.2	32.6	43.1	35.7	30.1

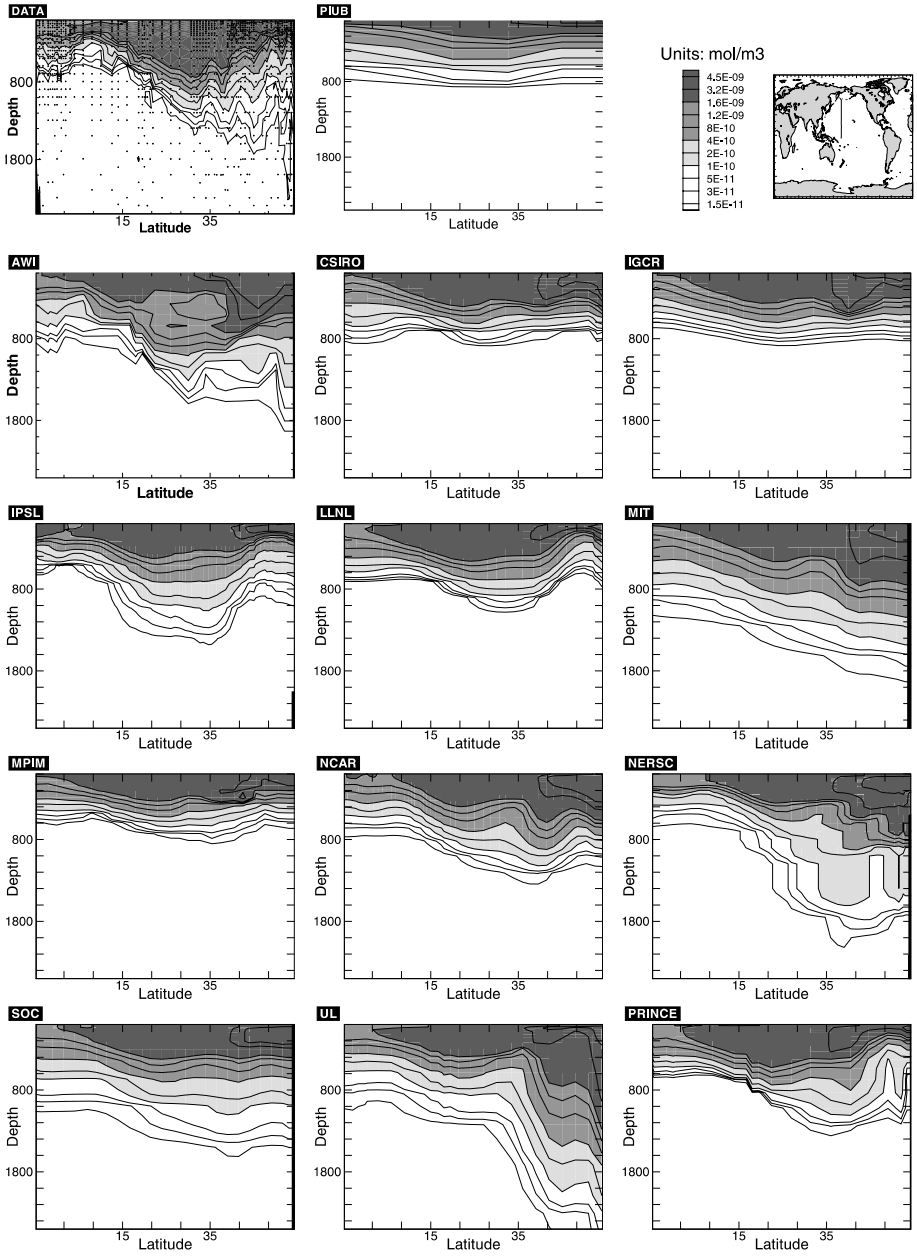

Fig. 3. CFC-11 concentration along the P13 section (1992). Units: mol/m^3.

4.3. North Atlantic

Substantial intermediate and deep waters are formed in the North Atlantic. The observed CFC-11 distribution in the Eastern North Atlantic along the WOCE NA20W section (in 1993) (Castle et al., 1993), provides insight regarding subsurface ventilation of the subtropical and subpolar

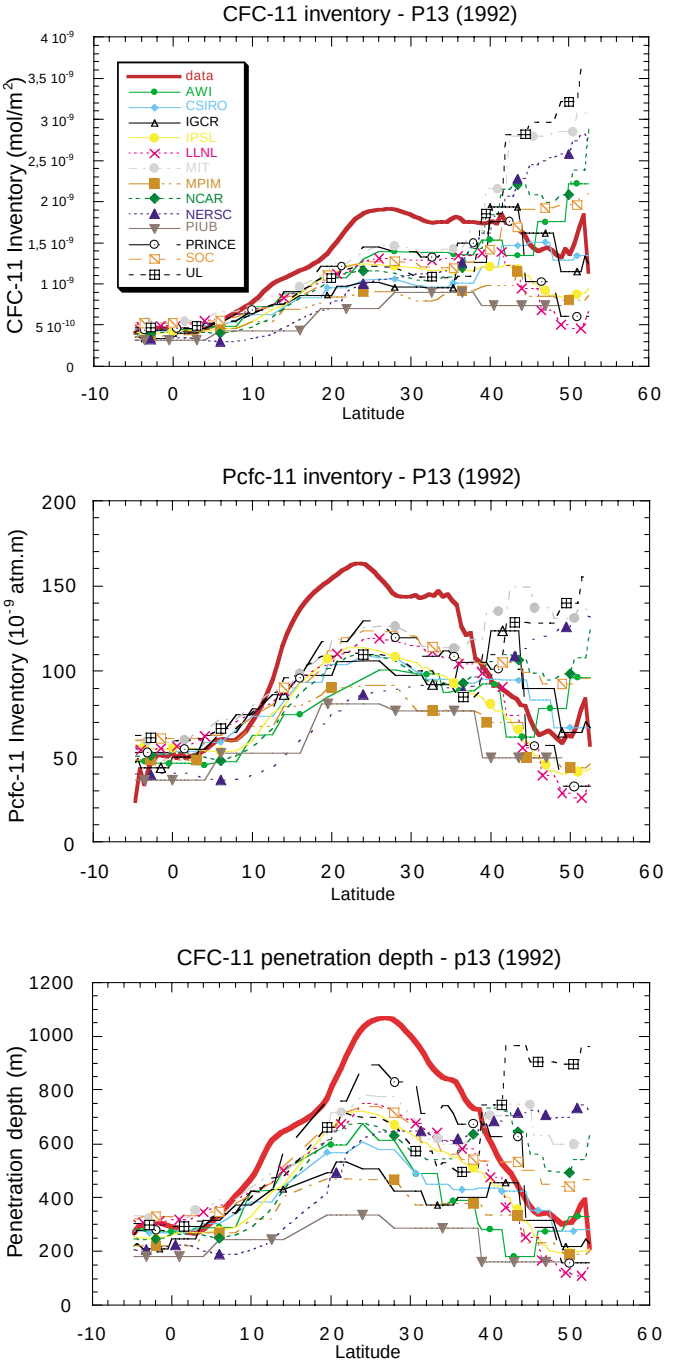

Fig. 4. CFC-11 and PCFC-11 verticl inventories and penetration depths along the P13 section.

gyres (Fig. 5). In that region, formation of a variety of mode waters by winter convection (McCartney and Talley, 1982) produces a uniform vertical CFC distribution below the seasonal thermocline (Doney and Bullister, 1992) to a depth that appears also to vary in time (Doney et al., 1998). Along this section, the mean observed CFC-11 penetration depth in subsurface increases

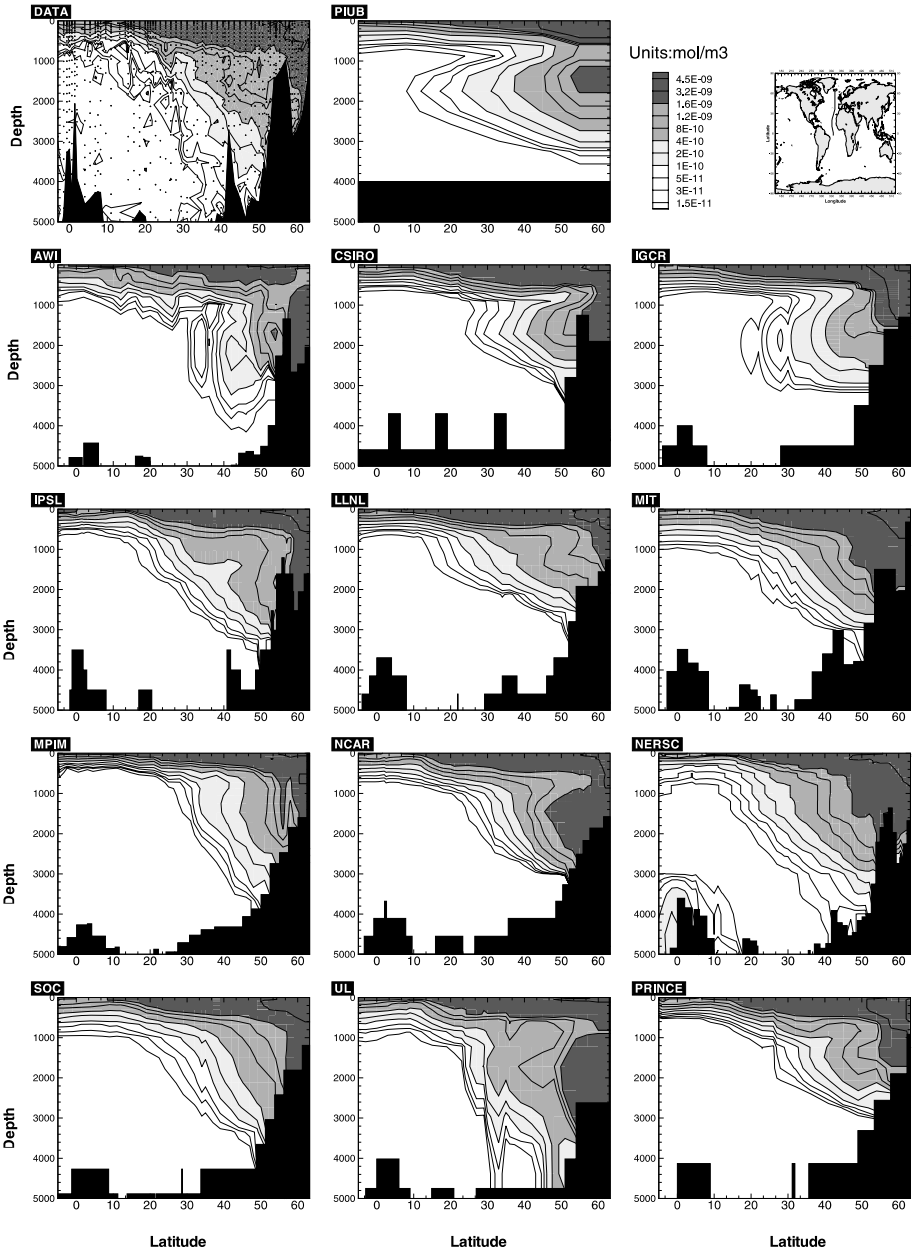

Fig. 5. CFC-11 concentration along the Na20w section (1993). Units: mol/m^3.

from 400 to 1000 m as one moves northward from 20°N (Fig. 6(c)), [1] which shows that CFC uptake is large in the North Atlantic subpolar gyre in stark contrast to its North Pacific counterpart. Although all models tend to show this increase, most of them underestimate the CFC-11 inventory and CFC-11 penetration depth in the subtropical gyre. Only two models (NERSC, MIT) slightly overestimate inventories and penetration depths in the subpolar gyre (Fig. 6). Four models (PIUB, MPIM, AWI, IGCR), have particularly low CFC-11 uptake in the subtropical gyre. Three of these models (MPIM, AWI, IGCR) are forced with annual means (Table 2), that does not allow to reproduce deep winter mixed layers and a realistic subduction that is known to be strongly seasonally aliased with the winter conditions (Williams et al., 1995).

The NA20W section is located in the eastern limit of the recirculation of the Labrador Sea Water (LSW) in the North Atlantic subpolar gyre (Talley and McCartney, 1982). Fig. 5 reveals observed CFC-11 concentrations that are elevated below 1000 m in the deep ocean due to renewal of North Atlantic Deep Water (NADW). We can assess in more detail the NADW ventilation characteristics, with its different components and source regions, from the zonal section at 24°N (Fig. 7) performed during the WOCE program (Peltola et al., 2001). The A24N section shows the well-known observed vertical distribution of CFCs within the Deep Western Boundary Current (DWBC), with two maxima along the continental slope (Molinari et al., 1992; Smethie, 1993; Rhein et al., 1995; Andrié et al., 1999). The deep maximum lies between 3000 and 4000 m depth, indicating the presence of Lower North Atlantic Deep Water (LNADW). The LNADW forms from the Denmark Strait Overflow Water (DSOW) and the Iceland–Scotland Overflow Water (ISOW). These source waters mix after flowing over the Greenland–Iceland–Scotland Ridge. The shallow maximum, between 1500 and 1800 m, corresponds to the Upper North Atlantic Deep Water (UNADW). The rate of formation and properties of the UNADW vary on a decadal timescale (Pickart, 1992). The classical component of UNADW is the LSW. The UNADW signal observed on A24N in 1998, is an upper LSW component, which is believed to have been ventilated in the early 1980s from south of the classical formation region, outside the western Labrador sea gyre (Pickart, 1992). The DWBC is also linked with some tight recirculation which is involved in ventilation of the ocean interior (Hogg and Stommel, 1985; Pickart and Hogg, 1989). Along A24N, significant CFC-11 concentrations are observed in the deep ocean interior, as far west as 40°W for the UNADW component and 50°W for the LNADW.

The AWI model is the only one that succeeds in producing the two subsurface CFC maxima in the western Atlantic. The other models produce only one CFC maximum corresponding to modeled NADW. The structure and position of this simulated maximum, recently ventilated NADW, varies substantially. The simulated depth of this maximum varies by hundreds of meters among the models. Generally, it lies between the depth of the two maxima on the observed section at 24°N, except for the LLNL and SOC models, where it is significantly shallower, and the isopycnal model (NERSC), where it lies at the bottom of the ocean. Longitudinally, the single maximum is sometimes located a few tens of degrees of longitude offshore in some models, thereby showing error in circulation pathway and increasing the volume of the deep interior ocean that is ventilated on a decadal timescale. All models have coarse resolution, thus the modeled DWBC spans at least few grid points, and is wider than in the real ocean. In the AWI model ocean

[1] In Fig. 6, the integration is limited to 1100 m depth in order to restrain the analysis to SPMW.

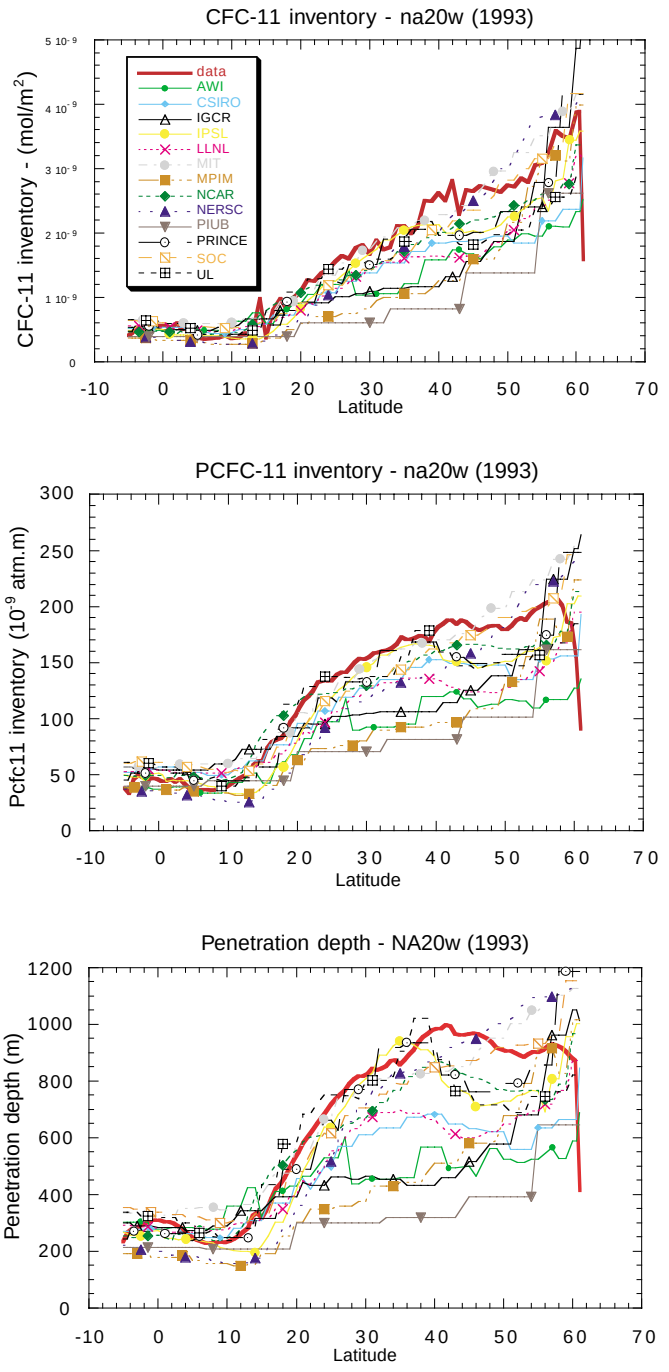

Fig. 6. CFC-11 and PCFC-11 vertical inventories and penetration depths along the Na20w section. Integration is limited to 1100 m depth in this calculation in order to restrain the analysis to SPMW.

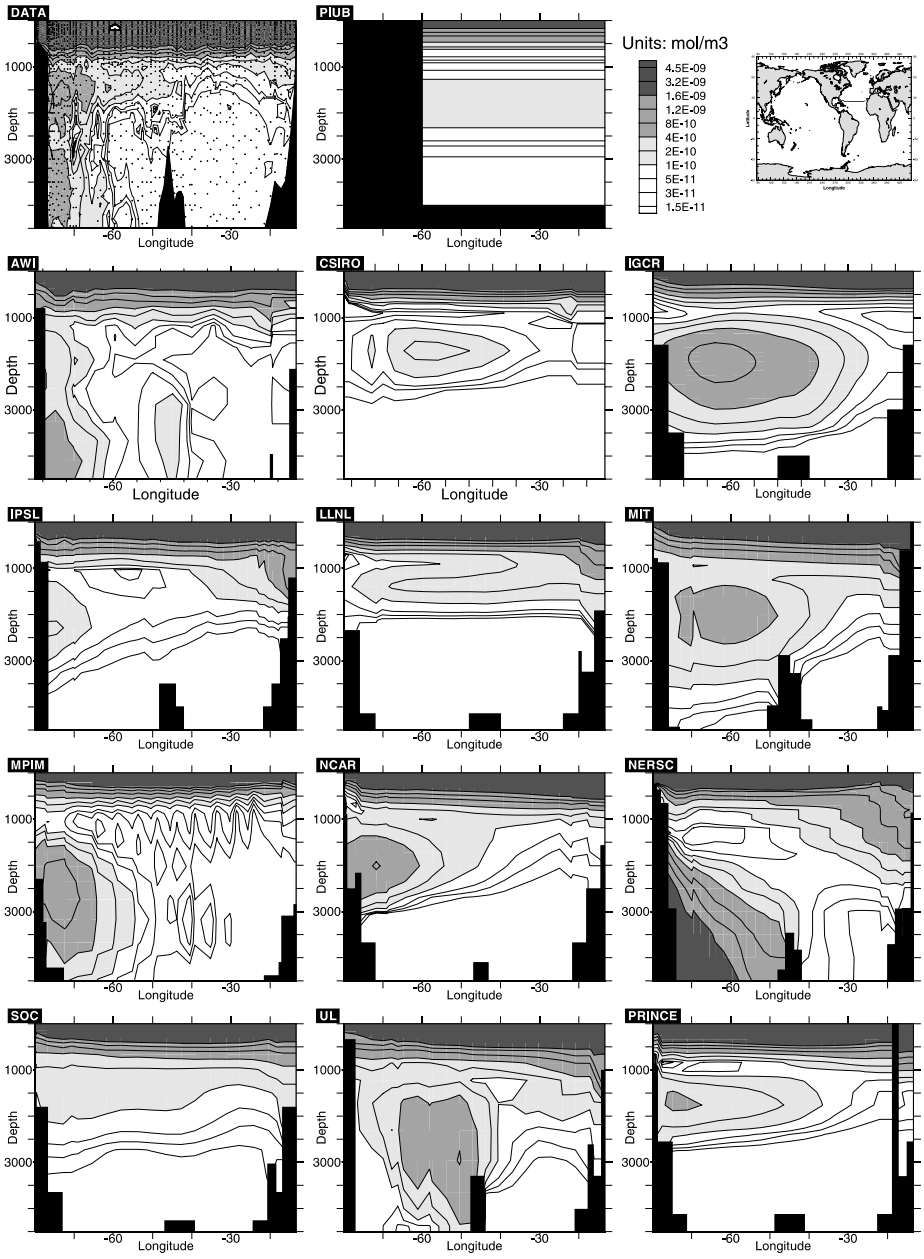

Fig. 7. CFC-11 concentration along the A24N section (data, 1998; models, 1997). Units: mol/m^3.

interior ventilation is too weak for the upper component, but too strong for the lower component, spreading too much into the ocean interior.

Having analyzed the vertical structure of CFC-11 within the DWBC, we now investigate the lateral spreading of the upper NADW component produced by the models. Weiss et al. (1985) have shown that at the time of the TTO survey in 1983, CFC-enriched water had already reached

the tropical Atlantic via the DWBC. The measurements presented on the $\sigma_{1.5} = 34.63$ kg/m^3 surface (≈ 1600 m) show a well-ventilated core of UNADW with a significant CFC-11 concentration of 0.05 pmol/kg having reached the western equatorial Atlantic (Fig. 8). The corre-

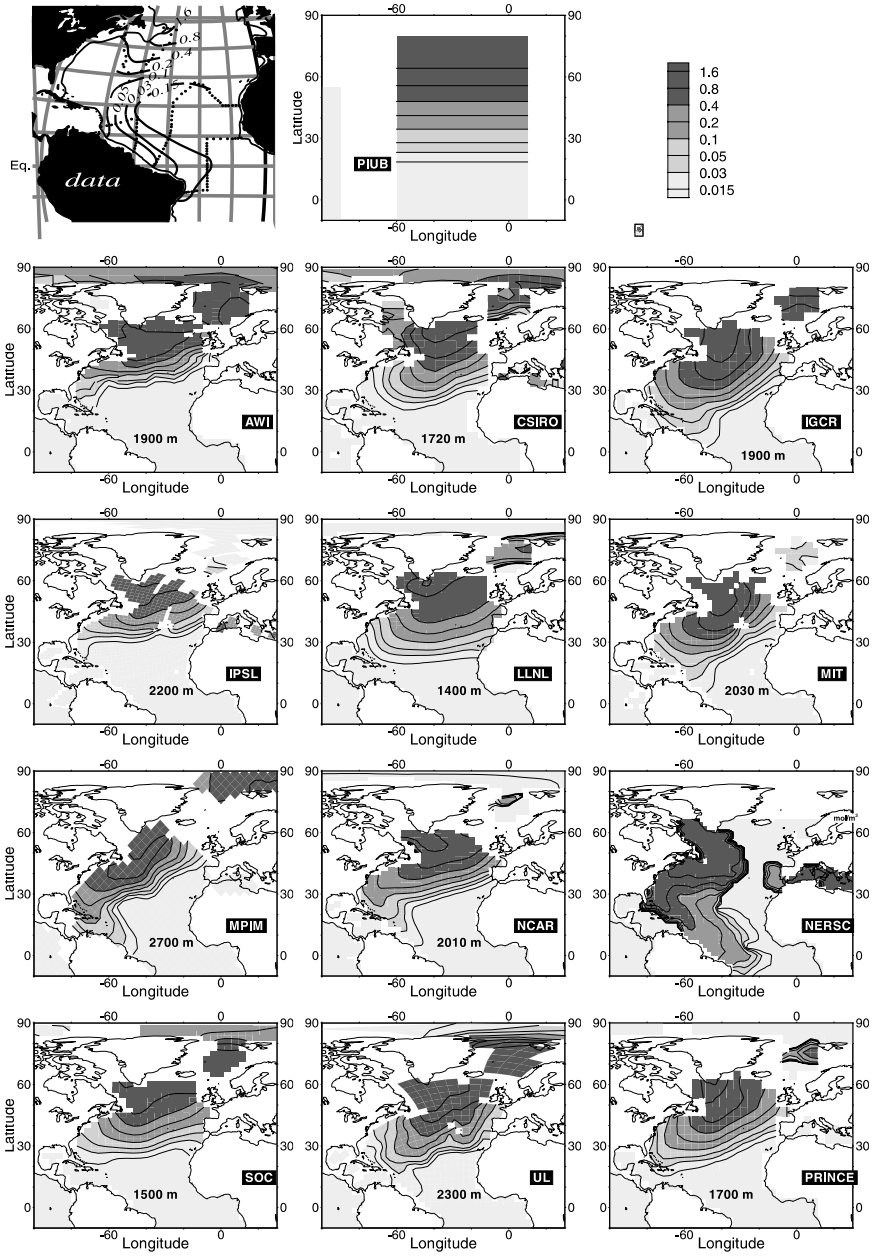

Fig. 8. Data: CFC-11 concentration on the $\sigma_{1.5} = 34.63$ isopycnal surface in 1983. Units: picomol/l, from Weiss et al. (1985). Models: CFC-11 concetration at the depth (or σ level for NERSC) of the core of UNADW of the models in 1983. Units: picomol/l.

sponding model results are shown on the depth (or for the NERSC model, along the σ level) that coincide with the NADW core in each model (Fig. 8). Close to the source region in the north, models have CFC-11 concentrations similar to the observations (0.8–1.6 picomol/l). Nearer the equator, the *Z*-coordinate models underestimate CFC-11 concentrations in the western boundary outflow, whereas the isopycnal layer model, NERSC, overestimates it. Two of the *Z*-coordinate models (NCAR and MPIM) succeed in producing CFC-11 rich water (>0.03 pmol/l) as a well-defined DWBC along the coast of South America, whereas others (CSIRO, MIT, LLNL, UL and PRINCE) unrealistically spread the CFC-11 signal into the interior of the deep ocean. In these models, the tracer spreads into the ocean interior by lateral diffusion although the velocity field deviates from a pure equatorward steering.

4.4. Southern Ocean

Fig. 2 reveals dramatic differences between models for the cumulative flux in the Southern Ocean. Two sections provide a more in-depth view of model performance in the Southern Ocean: the AJAX section, which was taken in 1983–1984 in the South Atlantic Ocean along the Greenwich meridian from Africa to Antarctica (Weiss et al., 1990; Warner and Weiss, 1992) (Fig. 9); and the WOCE P15s section (WOCE Data Products, 2000), which was taken in 1996 in the South Pacific Ocean, from the Equator to the region surrounding the Ross Sea (Fig. 10). The observed CFC-11 distribution along these two sections reveals the signature of the principal water masses of the Southern Ocean. The sharp subsurface tracer penetration down to approximately 1000 m depth occurring between 55°S and 40°S reflects the formation of Subantarctic Mode Water (SAMW). At greater depths, low CFC concentrations south of the ACC reveal weakly ventilated Circumpolar Deep Water (CDW). Nearer the bottom, higher CFC-11 concentrations indicate recently ventilated Antarctic Bottom Water (AABW). The source of AABW for P15s is the Ross Sea and for AJAX it is the Weddell Sea and the Amery Ice shelf (Orsi et al., 1999). These bottom water CFC-11 concentrations are typically 100 times less than those in the surface waters, but concentrations remain significantly higher than the detection limit (0.01 picomol/l), and thereby clearly indicate recent ventilation. The CFC-11 vertical inventory along these sections clearly shows how SAMW ventilation is more important than AABW ventilation in some respects to anthropogenic gases uptake in the Southern Ocean (Fig. 11). The standard non-linear CFC concentration color bar in the full depth section plots (Figs. 9 and 10) emphasizes the differences in the deep waters, but in terms of inventory, the SAMW dominates.

Model results differ substantially along these two sections. Sea-surface CFC-11 concentrations are similar to those observed, but the tracer concentrations in the ocean's interior differ substantially among models. Some models succeed in reproducing the sharp subsurface penetration of the CFCs at the subantarctic front associated with the SAMW ventilation (AWI, CSIRO, IPSL, LLNL, MIT, NCAR, SOC, PRINCE and NERSC). In other models (MPIM, IGCR and UL) CFC-11 penetration is less realistic, extending vertically into the Circumpolar Current, but not diagonally (along isopycnals) towards the subtropics. The general CFC-11 distribution in the SAMW subduction region along the AJAX section in the Atlantic Ocean (between 55°S and 40°S) is captured by several of the models, with simulated penetration depths and inventories that are close to that observed (800 m), though there is a tendency in several models (MPIM, LLNL, CSIRO, PIUB, and PRINCE) for these quantities to be on the low side (Fig. 11). In this

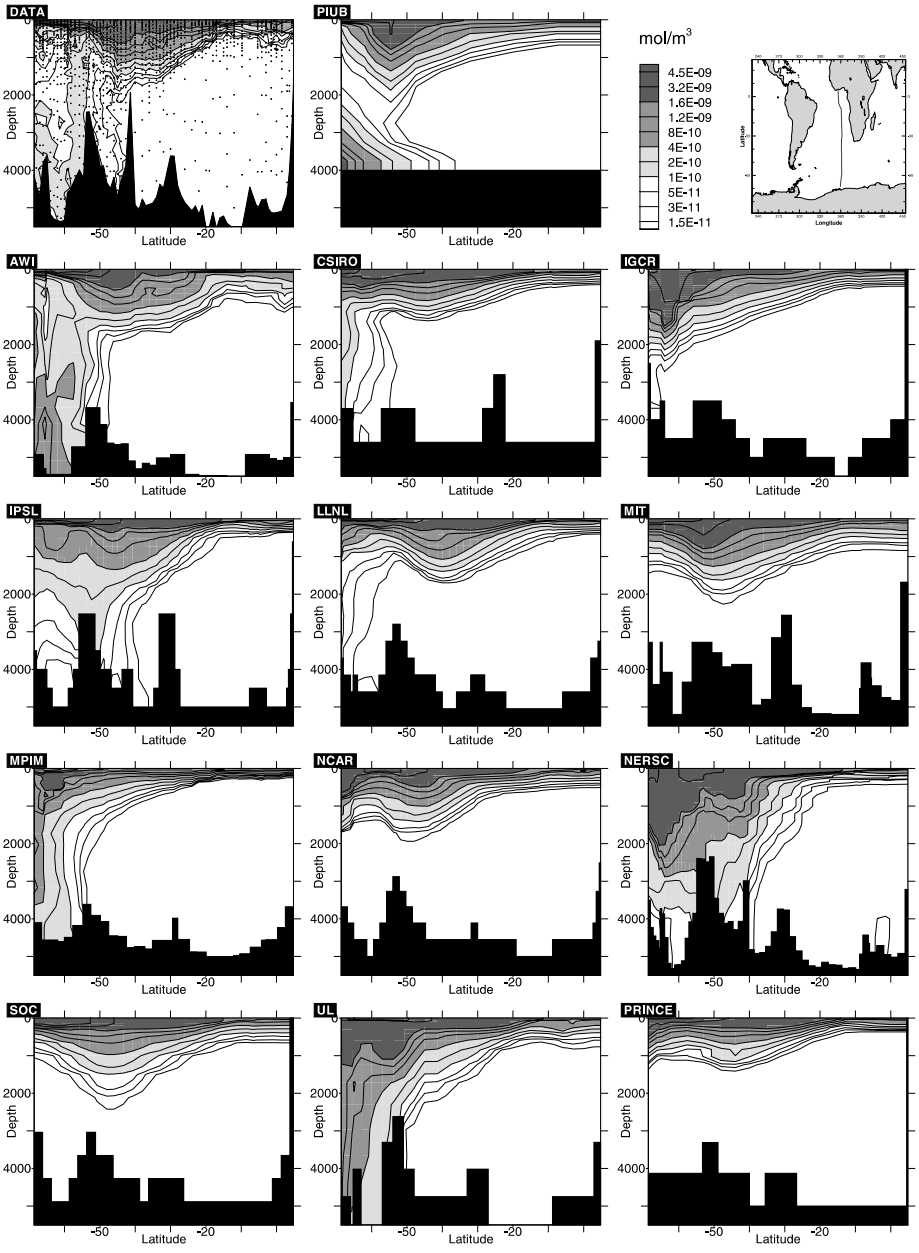

Fig. 9. CFC-11 concentration along the AJAX section (1983). Units: mol/m^3.

region, modeled CFC-11 distribution are backed by the MPIM model which has a weak SPMW ventilation and low CFC-11 inventory, and the NERSC model that overestimates the CFC-11 inventory and penetration depth. The observed CFC-11 penetration depth along P15s section reaches 1000 m in the SAMW subduction region (between 60°S and 50°S), and is deeper than that observed in the Atlantic Ocean along the AJAX section (Fig. 11). Compared to the

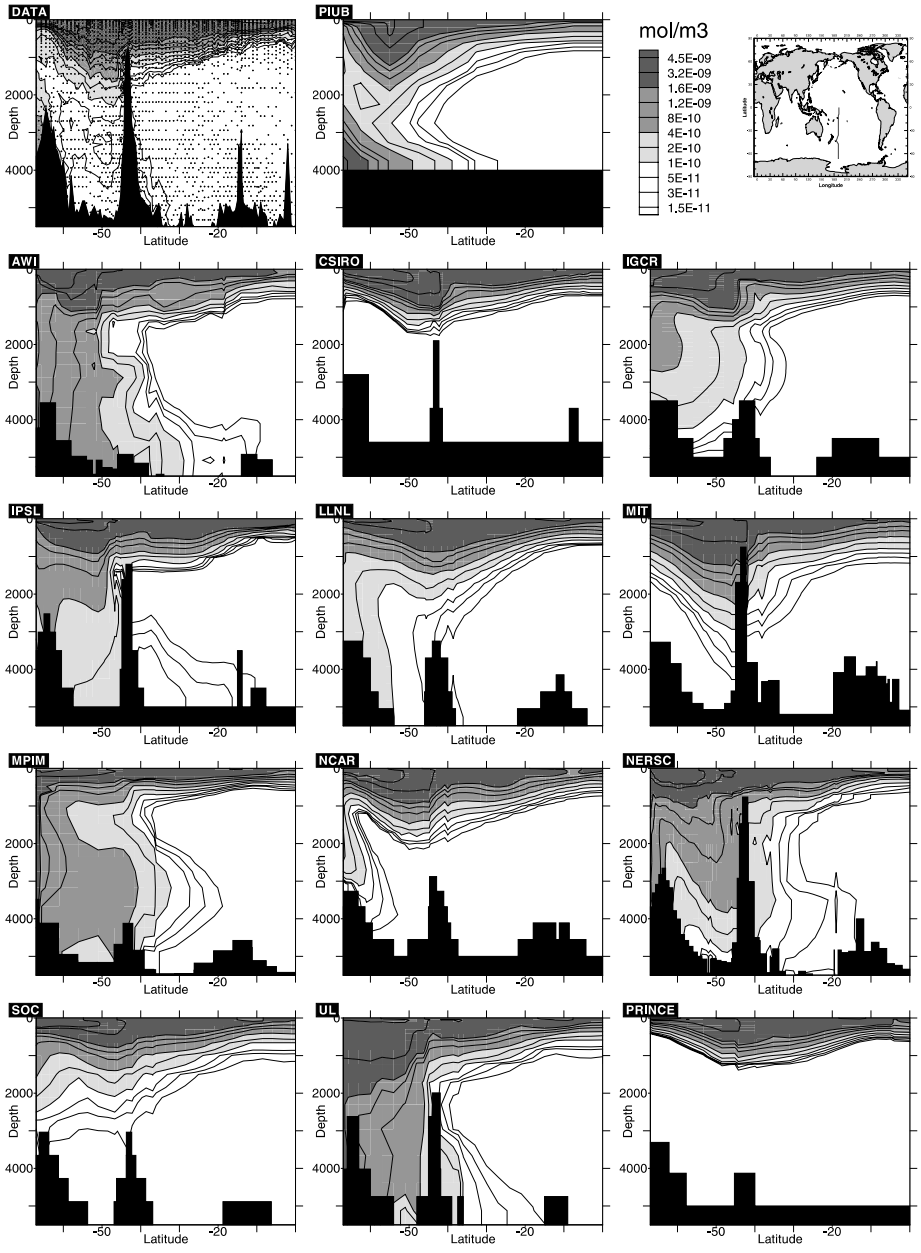

Fig. 10. CFC-11 concentration along the P15s section (1996). Units: mol/m^3.

observations, most of the models have similar or too large CFC-11 inventories and penetration depth along P15s. Exceptions are the CSIRO, LLNL, and PRINCE models which underestimate the CFC-11 inventory between 60°S and 50°S. The CSIRO and LLNL models have a realistic magnitude for the maximum CFC-11 inventory, but it is located further north between 50°S and 35°S.

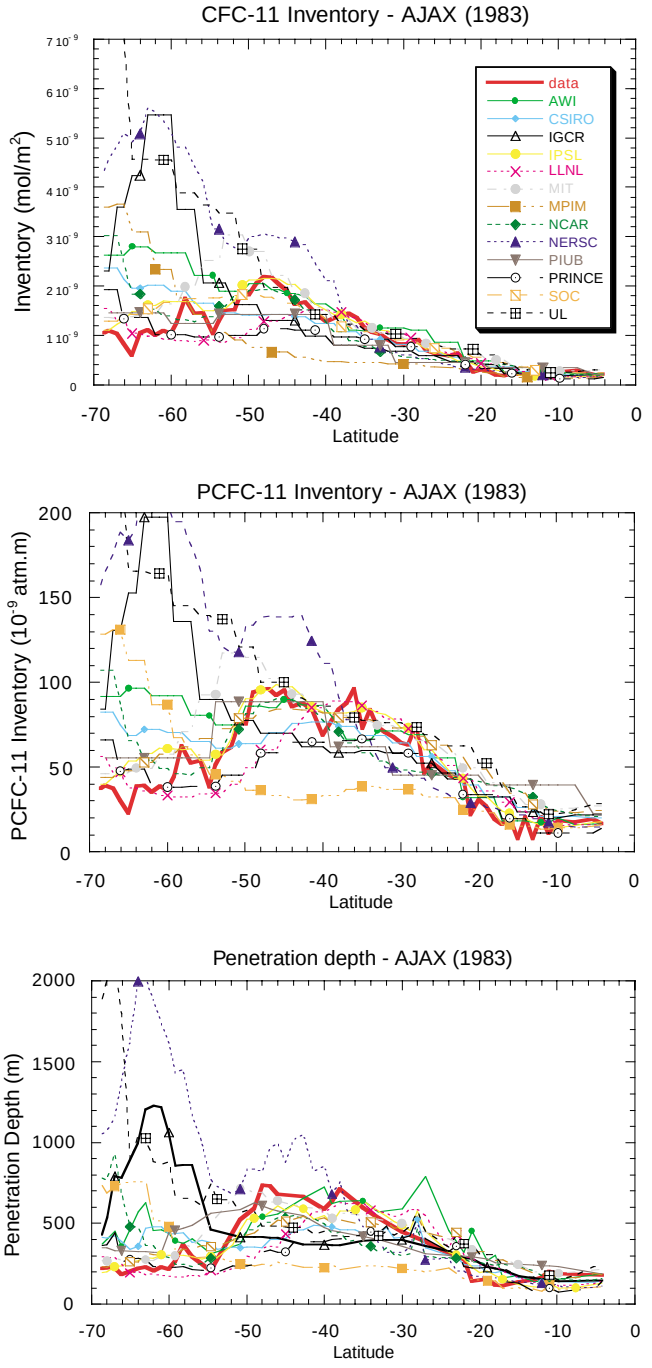

Fig. 11. CFC-11 and PCFC-11 vertical vertical inventories and penentration depths along the AJAX and P15S sections.

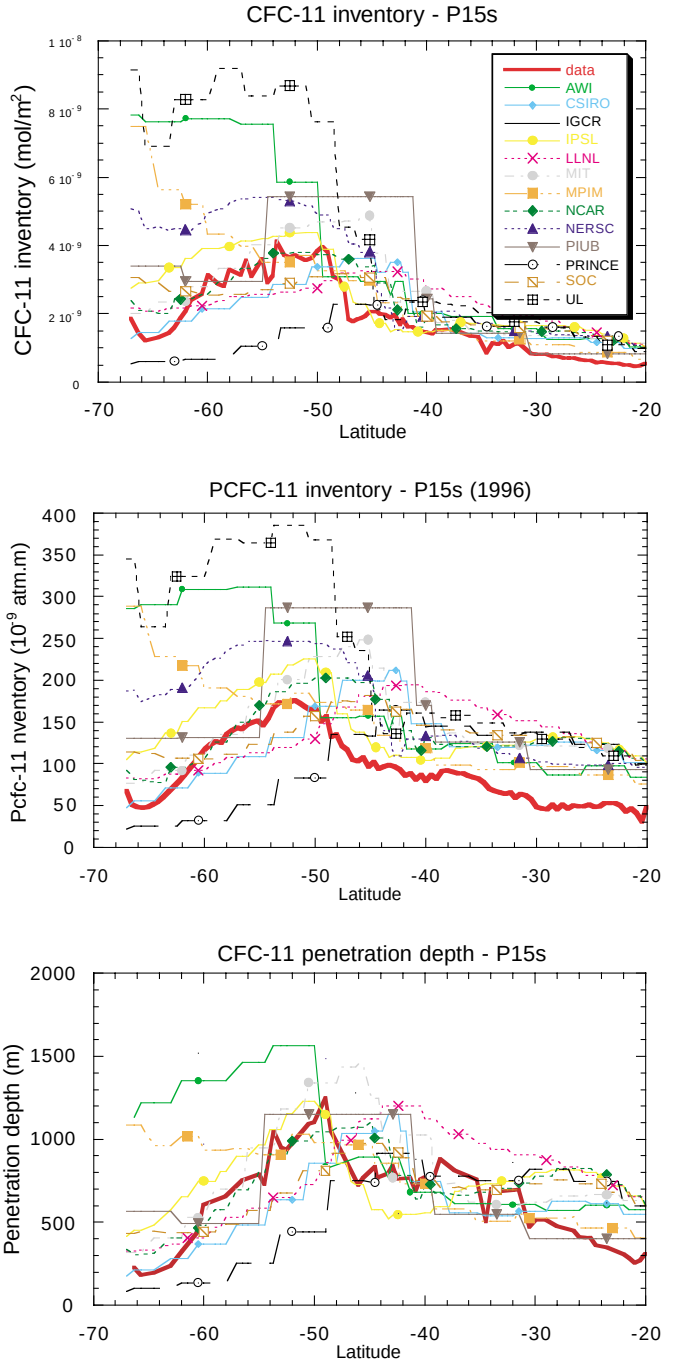

Fig. 11. (Continued).

AABW ventilation also differs dramatically among the models. The inverse model (AWI), the isopycnic model (NERSC) and the four models that are coupled to sea-ice models (LLNL, MPIM, UL, PIUB) all show, on both sections, significant CFC concentrations at the bottom due to AABW ventilation. However their skill varies: the AABW CFC-11 concentrations are realistic in the LLNL model, but overpredicted by more than a factor of 10 in the five other models mentioned above. Ocean models that are not coupled to a sea-ice model, generally produce a weaker ventilation of AABW, and CFC-11 concentrations that are too low in the deep Southern Ocean. Exceptions are the CSIRO model on AJAX and the NCAR, IPSL and IGCR models on P15s, which produce significant CFC-11 concentrations in the deep Southern Ocean.

Recent analysis of the new CFC WOCE data set in the deep Southern Ocean (Orsi et al., 1999) provides a large-scale picture that allows us to assess the simulation of AABW formation. Bottom maps on the abyssal layer show newly formed CFC-rich bottom water sinking from source regions located around Antarctica: in the western Weddell Sea, around the Amery basin (50–100°E), off Wilkes Land (120–160°E) and in the Ross Sea (Fig. 12). We compared the Orsi et al. data analysis with simulated CFC-11 concentration averaged over year 1990 at 2800 m depth (Fig. 12). The latter is indicative of simulated AABW ventilation characteristics close to Antarctica. Analogous maps at different times or depths in the abyssal ocean provide the same qualitative information. Models exhibit dramatic differences in AABW ventilation. The inverse model (AWI) and ocean models coupled with a sea-ice model form AABW at several locations around Antarctica similar to observed patterns, although of different intensity. Our previous comparison along P15s and AJAX sections revealed that the CFCs concentrations in the bottom layer of these models are for the most part too high, except for the LLNL model. The isopycnal model (NERSC) exhibits high deep CFC concentration and deep water ventilation all around Antarctica. AABW ventilation in the other models is weaker, with source regions either exclusively in the Weddell Sea (CSIRO, PRINCE), or in both the Weddell and Ross Seas (IGCR, NCAR and SOC). Unlike other models, the MIT and IPSL models do not show substantial bottom water ventilation around Antartica. Instead the MIT model forms AABW only in Drake Passage, and the IPSL model ventilate the deep Southern Ocean throughout the ACC.

5. Discussion

Global uptake of CFC-11 predicted by the OCMIP-2 models varies by $\pm 30\%$ around the mean. Thus establishing an observed global CFC inventory, with reasonable accuracy, would provide an important constraint for global OGCMs. Furthermore, a linear relationship in the trend of global CFC uptake exists among all models. Surface Ocean CFC concentrations equilibrate rapidly with the atmosphere (Doney and Jenkins, 1988) and all models are forced to follow the same temporal CFC increase in the atmosphere. Hence global uptake of CFCs is controlled by a global subduction rate whose magnitude differs for each model. The differences between the models and the observations are not due to biases in model-simulated temperature because model evaluation with both CFC-11 and PCFC-11 inventories along sections lead to the same conclusions. Thus, these differences must be ascribed to different model circulation fields. Differences in the global CFC-11 budget among models derive mainly from the Southern Ocean, where CFC uptake is concentrated in the SAMWs. In that region zonally integrated fluxes are largest and models differ significantly.

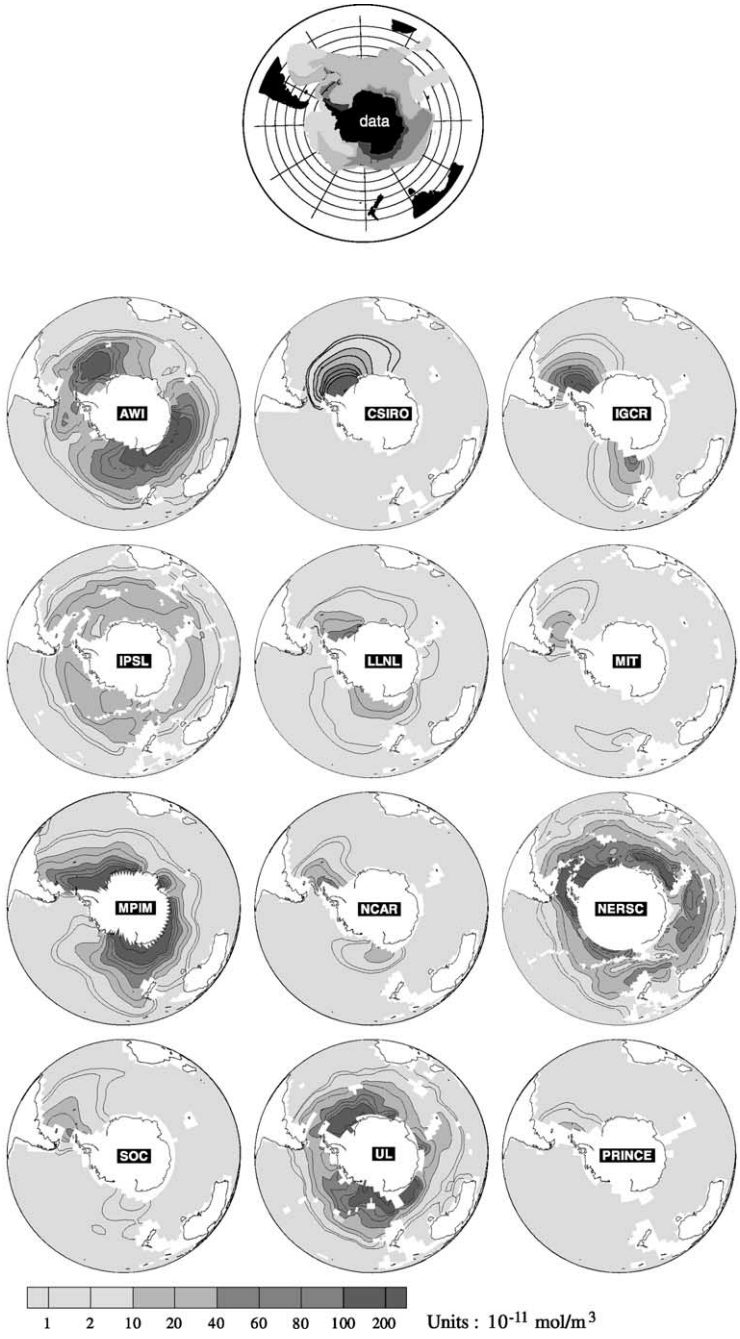

Fig. 12. Data: CFC-11 concentration in AABW; $\sigma > 28.27$ kg/m^3; Atlantique (1987) and Pacifique and Indian (1993). Units: Picomol/l – adapted from Orsi et al. (1999). Models: CFC-11 concentration at 2800 m depth. Units: 10^{-11} mol/m^3.

For instance, our model-data comparison along sections reveals that the UL and NERSC models absorb the most CFC-11 globally and are ventilated too strongly in the Southern Ocean. Conversely the PRINCE model has the lowest global CFC uptake and correspondingly weak ventilation in the Southern Ocean, particularly within the SAMW.

Some of the differences in Southern Ocean ventilation can be related to general physical forcing, while others are obviously more closely related to the physics or model parameterizations (Table 2). The meridional distribution of the uptake of CFCs in the Southern Ocean appears to be closely related to the parameterization of the lateral subgrid-scale mixing in the models. Most of the models without isopycnal diffusion (IGCR, MPIM, PIUB) exhibit maximum uptake south of 60°S (Fig. 2). On the other hand, all the depth coordinate models with lateral diffusion oriented along isopycnal surfaces exhibit maxima located closer to the subantarctic front, north of 60°S. The lateral mixing parameterization is crucial for SAMW subduction and ventilation. Subsurface ventilation in the Southern Ocean is very sensitive to the lateral subgrid scale mixing parameterization (Danabasoglu et al., 1994; Hirst and Cai, 1994; England, 1995; Duffy et al., 1997; Guilyardi et al., 2001). Models with horizontal mixing (IGCR, MPIM, UL, PIUB) show particularly unrealistic subsurface ventilation. They fail to produce substantial SAMW ventilation due to their inadequate isopycnal subduction at the base of the mixed layer. The other models, which have a lateral mixing oriented along isopycnal surfaces, produce more realistic SAMW ventilation. The resulting sharp vertical penetration of CFC-11 that occurs near the subantarctic front (55°S–45°S) is correlated with the more realistic low CFC-11 concentrations in the CDW (Figs. 9 and 10). The isopycnal model (NERSC) simulates excessive CFC-11 uptake all around the Antarctic continent. When deep convection occurs in the NERSC model, isopycnals simultaneously outcrop in the mixed layer. Therefore, the near-vertical isopycnals in the Southern Ocean allow excessive CFC to penetrate into the ocean interior.

Unlike the meridional distribution of CFC uptake, its longitudinal distribution shows no obvious relationship to model configuration or parameterizations. It is more likely that longitudinal variations in CFC uptake are controlled by the buoyancy forcing of the models. The primary sources of SAMW are mainly located in the Indian and Pacific sectors of the Southern Ocean (McCartney, 1982; Speer et al., 1997). Thus, models that have their maximum of CFC uptake located in the Pacific and Indian sectors of the Southern Ocean (IPSL and SOC) are more realistic in this regard. However, the location of the CFC-11 flux maxima (convection regions) is not the only important factor for intermediate water ventilation. Advection also plays a crucial role. Part of the mode water formed in one basin is later exported into another basin (Speer et al., 1997). Our CFC simulations reveal this tendency. For instance, the CSIRO model takes up more CFC-11 than does the SOC in the Southern Atlantic Ocean. Yet the CFC-11 penetration depth and inventory along the AJAX section in the Atlantic Ocean, are both larger for SOC than for CSIRO (Fig. 9). The formation (convection) regions of SAMW are now quite well established, and global basin subduction rates have been calculated. Unfortunately, the location of where SAMW is subducted is poorly understood (Speer et al., 1997). Thus it is difficult to evaluate the models further in this regard. CFC observations are useful for evaluating a model's ventilation characteristics, but they cannot constrain the origin of the ventilation.

The CFC-11 simulations also offer the opportunity to evaluate modeled formation and ventilation of AABW. Shelf-edge processes play a major role in the formation of deep and bottom waters in the Southern Ocean (Foster and Carmack, 1976). Since the models lack the spatial

resolution to resolve shelf-edge processes, they also tend to resort to unrealistic open-ocean convective processes to simulate deep and bottom ventilation (Goosse et al., 2001). However, coupling an ocean model to a sea-ice model appears to produce a more realistic pattern of model AABW source around Antarctica. Of all the forward models tested during OCMIP-2, only those coupled to a sea-ice model exhibit the recent ventilation by AABW in all three sectors of the Southern Ocean around Antarctica seen in a recent synthesis of observations by Orsi et al. (1999). These models also tend to overestimate this production. Thus including a sea-ice model or reasonable freshwater fluxes are necessary conditions for producing a realistic spatial distribution of the AABW formation region. Also model parameterizations for subgrid-scale mixing or salt rejection play an important role in propagating recently formed AABW. All models Coupled to a sea-ice model offer improved AABW source distribution, yet all but one of them simulate bottom water CFC-11 concentrations that are too high. The LLNL model, has clearly the most realistic CFC-11 concentrations in the bottom water of the Southern Ocean (Figs. 9, 10 and 12). The GM parameterization in these models helps stratify the deep Southern Ocean (England, 1995; Hirst and McDougall, 1996), but it is the treatment of brine rejected during sea-ice formation that distinguishes this model from others. In order to simulate concentrated brine plumes, the LLNL model transports salt, but not other tracers, downward during brine rejection (Duffy et al., 1997). Thus convection is reduced as is CFC-11 uptake in this region (Caldeira and Duffy, 1998). Still this parameterization is not the only mean for improving the representation of bottom water ventilation in these coarse resolution models. Additional sensitivity tests carried out by two OCMIP-2 modeling groups have shown that specific bottom boundary layer parameterizations may further contribute to an improvement in the propagation of AABW in the models (Campin and Goosse, 1999; Doney and Hecht, in press).

In the northern hemisphere, the regions of high CFC-11 uptake are the North Atlantic and Northwestern Pacific. The large-scale meridional structure of the subsurface ventilation of the subtropical region of these oceans appears adequate in all of the models. The simulated penetration of CFC-11 into subsurface layers does not seem to be improved by incorporating a more sophisticated mixed-layer parameterization. For instance, NCAR uses the KPP parameterization, but has a weaker vertical penetration than the Princeton model which has no mixed-layer model. This result is consistent with large-scale water mass properties being much more dependent on the surface forcing than on the surface boundary layer mixing scheme (Large et al., 1997). Simulated CFC-11 and PCFC-11 inventories and penetration depths are systematically too low, especially along the WOCE P13 section located near the STMW formation region in the Pacific. As all simulated PCFC-11 inventories are too low compared to the observations, it indicates a systematic shortcoming in the model circulation fields. Perhaps, mesoscale eddies, which are not resolved by any of the OCMIP-2 models, play an important role in ventilating the subtropical gyre.

Model performance concerning the ventilation of the subpolar subsurface gyre differs between basins. In the North Atlantic, the simulated CFC-11 uptake has a reasonable meridional structure, but is too low compared to the observations in all models but two. Lack of spatial resolution may partially explain that systematic bias. On the other hand, in the Northwestern Pacific, some models do succeed in reproducing the observed large-scale meridional structure of the CFC-11 uptake, with smaller inventories and penetration depths in the subpolar gyre. Other models (MIT, SOC, NERSC, NCAR and UL) overestimate the uptake of CFC-11 in the North Pacific subpolar

gyre. In the North Pacific, the shallow penetration depth simulated in some of the models may also be partially due to the poor representation of the marginal seas (Sea of Okhotsk) and exchange through straits.

Our results reveal shortcomings in the ability of many models to simulate the ventilation of the deep water in the Northern hemisphere. In most models, deep water formation in the Northern hemisphere is localized in the Irminger Sea and in the Greenland–Iceland–Norwegian (GIN) seas (Fig. 2). Conversely in the MIT, NERSC, and UL models, maximum uptake occurs in the north Atlantic subpolar gyre, in the Labrador Sea (Fig. 2). This coincides better with formation of UNADW in the real ocean (McCartney and Talley, 1982). The vertical structure of the recently ventilated NADW (Fig. 7) is not clearly related to the formation region in the models. Only the adjoint model (AWI) produces the two separate ventilated branches of NADW (UNADW and LNADW), as observed. Modeled deep water formation in the GIN seas does not produce a distinct, recently ventilated core in the DWBC because overflow from the Nordic seas is poorly simulated in coarse resolution models, particularly if they do not include any specific parameterization of dense water overflow over the sills (Beckmann and Döscher, 1997; England and Holloway, 1998; Redler and Dengg, 1999).

The simulated lateral spreading of CFC-11 in the DWBC also reveals shortcomings in the modeled thermohaline circulation on the decadal timescale. Some of the models have well-defined DWBC (e.g. AWI, IPSL, MPIM, NCAR and NERSC) whereas others (e.g. CSIRO, LLNL and MIT) produce excessive ventilation into the ocean interior. All models, except for the NERSC isopycnal model, produce CFC-11 concentrations in the DWBC that are too low. Thus transport of tracer is too weak in the cold branch of the thermohaline circulation of these coarse resolution *Z*-coordinate models. The unrealistic vertical structure of NADW ventilation may also explain why the modeled DWBC is too slow. With a higher-resolution model, Böning et al. (1996) show that if dense overflow from the Greenland and Norwegian Seas is inadequate, then this also reduces the total export of NADW from the subpolar gyre. Further reduction of southward transport of CFC-11 in coarse resolution models is due to artificial upwelling in the DWBC caused by the crude representation of the lateral boundary layer used in these models (Huck et al., 1999). This model artifact results in diluting the CFC signal due to mixing with CFC-poor deeper water, and thereby creates an unrealistic shortcut in the modeled thermohaline circulation. Such artificial upwelling is commonly found in coarse-resolution models using a horizontal lateral diffusion, which produces large diapycnal fluxes when isopycnals are tilted, the so-called "Veronis effect" (Toggweiler et al., 1989). Artificial upwelling persists when using isopynal diffusion and the GM parameterization, although its intensity is generally reduced along with the global meridional overturning (Lazar et al., 1999). It is then balanced by downward eddy-induced advection, which also tends to mix the tracer signal in the DWBC. The impacts of these shortcomings of the thermohaline circulation of coarse-resolution models will also have an impact on the simulated redistribution of carbon by the ocean.

6. Conclusion

Standard CFC-11 simulations were made in 13 coarse-resolution models so that uptake and transport of this tracer could be used as an evaluation tool for model performance, particularly

over decadal timescales. The range of the simulated global CFC-11 uptake is large (±30% about the mean result), mainly due to differences in the Southern Ocean. An observed CFC inventory would provide a useful benchmark for evaluating the decadal ventilation characteristics of global OGCMs. Observations and derived analysis products of CFC measurements from WOCE and some previous programs have been useful for testing the models. Our analysis of the Southern Ocean reveals that ocean models coupled with a sea-ice component model systematically provided more realistic patterns of AABW formation source region, than those without this component.

Nonetheless, the propagation of AABW into the interior of the ocean also depends on the parameterization of ocean physics. Models with a sea-ice component produced excess deep water formation in the Southern Ocean or indeed near the Bering strait (e.g. UL). An exception was the LLNL model with its specific parameterization for vertical redistribution of brine rejection during sea-ice formation. Models with lateral diffusion oriented along isopycnals that also include the GM eddy-induced velocity parameterization produce more realistic intermediate water ventilation in the Southern Ocean. However, models differ longitudinally in regions where SAMW is formed, probably because the lack of data allows modelers too much liberty in specifying Southern Ocean heat and fresh water fluxes. Therefore improving heat and fresh water flux climatologies in the Southern Ocean would help improve ocean models, as would new constraints for interannual and decadal climate variability in this region. In the northern hemisphere, all models underpredict the CFC-11 uptake in the subtropics and in the subtropical gyre of the Atlantic Ocean. As for NADW, only the adjoint AWI model succeeds in producing the two recently ventilated branches of NADW. Other models produce only one branch with related transport in DWBC being too sluggish, except in the NERSC isopycnal model where it is too rapid. Our standard OCMIP protocols and archive of CFC-11 and CFC-12 model output should be useful for continued evaluation of ocean model performance. More information about OCMIP can be found at http://www.ipsl.jussieu.fr/OCMIP.

Acknowledgements

We are grateful to Patrick Brockmann for the development of Global Analysis Package (GAP) used for the analysis performed in this paper.

References

Andrié, C., Ternon, J.F., Bourlès, B., Gouriou, Y., Oudot, C., 1999. Tracer distributions and deep circulation in the western tropical Atlantic during CITHER1 and ETAMBOT cruises, 1993–1996. J. Geophys. Res. 104, 21,195–21,215.

Beckmann, A., Döscher, R., 1997. A method for improved representation of dense water spreading over topography in Geopotential-coordinate models. J. Phys. Oceanogr. 27, 581–591.

Bleck, R., Rooth, C., Hu, D., Smith, L.T., 1992. Salinity-driven thermocline transients in a wind- and thermohaline-forced isopycnic coordinate model of the North Atlantic. J. Phys. Oceanogr. 22, 1486–1505.

Böning, C.W., Bryan, F.O., Holland, W.R., Doscher, R., 1996. Deep water formation and meridional overturning in a high resolution model of the north atlantic. J. Phys Oceanogr. 26, 1142–1164.

Boutin, J., Etcheto, J., 1997. Long-term variability of the air–sea CO_2 exchange coefficient: consequences for the CO_2 fluxes in the equatorial Pacific Ocean. Global Biogeochem. Cycles 11, 453–470.

Broecker, W.S., Ledwell, J.R., Takahashi, T., Weiss, R., Merlivat, L., Memery, L., Peng, T.H., Jahne, B., Munnich, K.O., 1986. Isotopic versus micrometeorologic ocean CO_2 fluxes: a serious conflict. J. Geophys. Res. 91, 10,517–10,534.

Broecker, W.S, Sutherland, S., Smethie, W., Peng, T.-H., Ostlund, G., 1995. Oceanic radiocarbon: separation of the natural and bomb component. Global Biogeochem. Cycles 9, 263–288.

Bryan, K., 1969. A numerical method for the study of the circulation of the world ocean. J. Comput. Phys. 4, 347–376.

Bullister, J.L., Weiss, R.F., 1983. Anthropogenic chlorofluoromethanes in the Greenland and Norwegian seas. Science 221, 265–268.

Caldeira, K., Duffy, P.B., 1998. Sensitivity of simulated CFC-11 distributions in a global ocean model to the treatment of salt rejected during sea-ice formation. Geophys. Res. Lett. 25, 1003–1006.

Campin, J.M., Goosse, H., 1999. Parameterization of density-driven downsloping flow for a coarse-resolution model in *Z*-coordinate. Tellus 51A, 412–430.

Castle, R.D., Wanninkhof, R., Bullister, J.L., Doney, S.C., Feely, R.A., Huss, B.E., Johns, E., Millero, F.J., Lee, K., Frazel, D., Wisegarver, D., Greeley, D., Menzia, F., Lamb, M., Beberian, G., Moore Jr., L.D., 1993. Chemical and hydrographic profiles and underway measurements from the Eastern North Atlantic during July and August 1993. NOAA Data Report ERL-AOML.

Danabasoglu, G., McWilliams, J.C., Gent, P.R., 1994. The role of mesoscale tracer transports in global ocean crirculation. Science 264, 1123–1126.

Doney, S.C., Bullister, J.L., 1992. A chlorofluorocarbon section in the eastern North Atlantic. Deep-Sea Res. 39, 1857–1883.

Doney, S.C., Bullister, J.L., Wanninkof, R., 1998. Climatic variability in upper ocean ventilation rates diagnosed using chlorofluorocarbons. Geophys. Res. Lett. 25, 1399–1402.

Doney, S.C., Hecht, M., in press. Antarctic bottom water formation and deep water chlorofluorocarbon distributions in a global ocean climatemodel. J. Phys. Oceanogr..

Doney, S.C., Jenkins, W.J., 1988. The effect of boundary conditions on tracer estimates of thermocline ventilation rates. J. Mar. Res. 46, 947–965.

Duffy, P.B., Caldeira, K., Selvaggi, J., Hoffert, M.I., 1997. Effects of subgrid-scale mixing parametrisations on simulated distributions of natural ^{14}C, temperature and salinity in a three-dimensional ocean general circulation model. J. Phys. Oceanogr. 27, 498–523.

Dutay, J.-C., 1998. Influence du mélange vertical et de la couche mélangée sur la ventilation de l'océan. Simulations numériques des traceurs transitoires tritium-helium-3 et CFCs avec le modèle OPA. Ph.D. Thesis, Univ. Pierre et Marie Curie.

England, M.H., 1995. Using chlorofluorocarbons to assess ocean climate model. Geophys. Res. Lett. 22, 3051–3054.

England, M.H., Hirst, A.C., 1997. Chlorofluorocarbon uptake in a world ocean model 2. Sensitivity to surface thermohaline forcing and subsurface mixing parameterizations. J. Geophys. Res. 102, 15,709–15,731.

England, M., Holloway, G., 1998. Simulations of CFC content and water mass age in the deep North Atlantic. J. Geophys. Res. 103, 15,885–15,901.

Esbensen, S.K., Kushnir, Y., 1981. The heat budget of the global ocean: an atlas based on estimates from marine surface observations. Rep. 29, Clim. Res. Inst., Oregon State Univ., Corvallis.

Foster, T.D., Carmack, E.C., 1976. Frontal zone mixing and Antarctic bottom water formation in the Southern Weddell Sea. Deep-Sea Res. 23, 301–317.

Gaspar, P., Grégoris, Y., Lefevre, 1990. A simple eddy-kinetic-energy model for simulations of the ocean vertical mixing: tests at station Papa and long-term upper ocean study site. J. Geophys. Res. 95, 16,179–16,193.

Gent, P.R., Willebrand, J., McDougall, T.J., McWilliams, J.C., 1995. Parameterizing eddy-induced tracer transports in ocean circulation models. J. Phys. Oceanogr. 25, 463–474.

Gnanadesikan, A., Slater, R.D., Sarmiento, J.L., in press. New production as a constraint on oceanic vertical exchange. Deep-Sea Res..

Goosse, H., Campin, J.M., Tartinville, B., 2001. The sources of Antarctic bottom water in a global ice-ocean model. Ocean Model. 3 (1–2), 51–65.

Goosse, H., Delersnijder, E., Fichefet, T., England, M.H., 1999. Sensitivity of a global coupled ocean-sea ice model to the parameterization of vertical mixing. J. Geophys. Res. 104, 13,681–13,695.

Goosse, H., Fichefet, T., 1999. Importance of ice-ocean interactions for the global ocean circulation: a model study. J. Geophys. Res. 104, 23,337–23,355.

Gordon, C., Cooper, C., Senior, C.A., Banks, H., Gregory, J.M., Johns, T.C., Mitchell, J.F.B., Wood, R.A., 2000. The simulation of SST, sea ice extents and ocean heat transport in a version of the Hadley Centre coupled model without flux adjustments. Climate Dyn. 16, 147–168.

Gruber, N., Sarmiento, J., Stocker, T., 1996. An improved method for detecting anthropogenic CO_2 in the oceans. Global Biogeochem. Cycles 10, 809–837.

Guilyardi, E., Madec, G., Terray, L., 2001. The role of lateral ocean physics in the thermal balance of a coupled ocean-atmosphere GCM. Clin. Dyn. 17, 589–599.

Haine, T., Gray, S., 1999. North Atlantic ventilation constrained by CFC observations. Int. WOCE Newslett. 35, 15–17.

Heinze, C., Maier-Reimer, E., Schlosser, P., 1998. Transient tracers in a global OGCM: source functions and simulated distributions. J. Geophys. Res. 103, 15,903–15,922.

Hirst, A.C., Cai, W., 1994. Sensitivity of a world ocean GCM to changes in subsurface mixing parametrization. J. Phys. Oceanogr. 24, 1256–1278.

Hirst, A., McDougall, T.J., 1996. Deep-water formation and surface buoyancy flux as simulated by a *Z*-coordinate model including eddy-induced advection. J. Phys. Oceanogr. 26, 1320–1343.

Hogg, N.G., Stommel, H., 1985. On the relation between the deep circulation and the Gulf Stream. Deep-Sea Res. 32, 1181–1193.

Huck, T., Weaver, A.J., Colin de Verdiere, A., 1999. On the influence of the parametrization of lateral boundary layers on the thermohaline circulation in coarse-resolution ocean models. J. Mar. Res. 57, 387–426.

Kraus, E.B., Turner, J.S., 1967. A one-dimensional model of the seasonal thermocline. 2. The general theory and its consequences. Tellus 19, 98–105.

Large, W.G., Danabasoglu, G., Doney, S.C., McWilliams, J.C., 1997. Sensitivity to surface forcing and boundary layer mixing in a global ocean model: annual mean climatology. J. Phys. Oceanogr. 27, 2418–2447.

Large, W.C., McWiliams, J.C., Doney, S.C., 1994. Oceanic vertical mixing: a review and a model with a nonlocal boundary layer parametrization. Rev. Geophys. 32, 363–403.

Lazar, A., Madec, G., Delecluse, P., 1999. The deep interior downwelling, the Veronis effect, and mesoscale tracer transport parameterizations in an OGCM. J. Phys. Oceanogr. 29, 2945–2961.

Madec, G., Delecluse, P., Imbard, M., Lévy, C., 1998. OPA8.1 ocean general circulation model reference manual. Notes du pôle de Modélisation de l'IPSL. 11.

Maier-Reimer, E., 1993. Geochemical cycles in an OGCM. Part 1. Tracer distributions. Global Biogeochem. Cycles 97, 645–677.

Maier-Reimer, E., Mikolajewicz, U., Hasselmann, K., 1993. Mean circulation of the Hamburg LSG OGCM and its sensitivity on the thermohaline forcing. J. Phys. Oceanogr., 731–757.

Marshall, J.C., Adcroft, A., Hill, C., Perelman, L., Heisey, C., 1997. A finite volume, incompressible Navier–Stokes model of the ocean on parallel computers. J. Geophys. Res. 102, 5753–5766.

Matear, R.J., Hirst, A.C., 1999. Climate change feedback on the future oceanic CO_2 uptake. Tellus 51B, 722–733.

McCartney, 1982. The subtropical recirculation of mode waters. J. Mar. Res. 40, 427–462.

McCartney, M., Talley, L.D., 1982. The subpolar mode water of the North Atlantic Ocean. J. Phys. Oceanogr. 12, 1169–1188.

Molinari, R.L., Fine, R.A., Johns, E., 1992. The deep western boundary current in the tropical North Atlantic Ocean. Deep-Sea Res. 39, 1967–1984.

Orr, J.C., 1999. Ocean Carbon-cycle Intercomparison Project (OCMIP). Phase 1 (1995–1997). IGBP/GAIM Report Series, Report #7.

Orr, J.C., Maier-Reimer, E., Micolajewicz, U., Monfray, P., Sarmiento, J.L., Toggweiler, J.R., Taylor, N.K., Palmer, J., Gruber, N., Sabine, C.L., Le Quéré, C., Key, R.M., Boutin, J., 2001. Estimates of anthropogenic carbon uptake from four 3-D global ocean models. Global Biogeochem. Cycles 15 (1), 43–60.

Orsi, A.H., Johnson, G.C., Bullister, J.L., 1999. Circulation, mixing, and production of Antarctic bottom water. Prog. Oceanogr. 43, 55–109.

Peltola, E., Lee, K., Wanninkhof, R., Feely, R., Roberts, M., Greeley, D., Baringer, M., Johnson, G., Bullister, J., Mordy, C., Zhang, J.-.Z., Quay, P., Millero, F., Hansell, D., Minnett, P., 2001. Chemical and hydrographic

measurements on a climate and global change cruise along 24°N in the Atlantic Ocean WOCE section A5R (Repeat) during January–February 1998, NOAA Data Report, ERL AOML-41.
Pickart, R.S., 1992. Water mass components of the North Atlantic deep western boundary current. Deep-Sea Res. 39, 1553–1572.
Pickart, R.S., Hogg, N.G., 1989. A tracer study of the deep Gulf stream cyclonic recirculation. Deep-Sea Res. 36, 935–956.
Qiu, B., Huang, R.H., 1995. Ventilation of the North Atlantic and North Pacific: subduction versus obduction. J. Phys. Oceanogr. 25, 2374–2390.
Redler, D., Dengg, J., 1999. Spreading of CFCs in numerical models of differing resolution. Int. WOCE Newslett. 35, 12–14.
Rhein, M., 1994. The deep western boundary current: tracers and velocities. Deep-Sea Res. 41, 263–281.
Rhein, M., Stamma, L., Send, U., 1995. The Atlantic deep western boundary current: water masses and transports near the equator. J. Geophys. Res. 100, 2441–2457.
Robitaille, D.Y., Weaver, A.J., 1995. Validation of sub-grid-scale mixing schemes using CFCs in a global ocean model. Geophys. Res. Lett. 22, 2917–2920.
Sabine, C.L., Key, R.M., Goyet, C., Johnson, K.M., Millero, F.J., Poisson, A., Sarmiento, J.L., Wallace, D.W.R., Winn, C.D., 1999. Anthropogenic CO_2 inventory of the indian ocean. Global Geochem. Cycles 13, 179–198.
Schlitzer, R., 1999. Applying the adjoint method for biogeochemical modeling: export of particulate organic matter in the world ocean. In: Inverse Methods in Global Biogeochemical Cycles, pp. 107–124.
Smethie, W.M., 1993. Tracing the thermohaline circulation in the western North Atlantic using chlorofluorocarbons. Prog. Oceanogr. 31, 51–99.
Smythe-Wright, D., Boswell, S., 1998. Abyssal circulation in the Argentine Basin. J. Geophys. Res. 103, 15,845–15,851.
Sonnerup, R.E., Quay, P.D., Bullister, J.L., 1999. Thermocline ventilation and oxygen utilization rates in the Subtropical North Pacific based on CFC distributions during WOCE. Deep-Sea Res. 46 (5), 777–805.
Speer, K., Rintoul, S., Sloyan, B., 1997. Subantarctic mode water formation by air–sea fluxes. Int. WOCE Newslett. 29, 29–31.
Stocker, T.F., Wright, D.G., Mysak, L.A., 1992. A zonally averaged, coupled ocean-atmosphere model for paleaclimate studies. J. Clim. 5, 773–797.
Suga, T., Takei, Y., Hanawa, K., 1997. Thermostad distribution in the North Pacific subtropical gyre: the general mode water and the subtropical mode water. J. Phys. Oceanogr. 27, 140–152.
Talley, L.D., McCartney, M.S., 1982. Distribution and circulation of Labrador Sea water. J. Phys. Oceanogr. 12, 1189–1205.
Toggweiler, J.R., Dixon, K., Bryan, K., 1989. Simulation of radiocarbon in a coarse-resolution world ocean model. 2. Distribution of bomb-produced carbon 14. J. Geophys. Res. 94, 8243–8264.
Walker, S.J., Weiss, R.F., Salameh, P.K., 2000. Reconstructed histories of the annual mean atmospheric mole fractions for halocarbons CFC-11, CFC-12, CFC-113, and carbon tetrachloride. J. Geophys. Res. 105, 14,285–14,296.
Wallace, D.W.R., Lazier, J.R.N., 1988. Anthropogenic chlorofluoromethanes in newly formed Labrador Sea water. Nature 332, 61–63.
Walsh, J., 1978. A dataset on northern hemisphere sea ice extent, 1953–1976. Rep. Glaciological data No. GD-2, World Data Center for Glaciology, pp. 49–51.
Wanninkhof, R., 1992. Relationship between wind speed and gas exchange over the ocean. J. Geophys. Res. 97, 7373–7382.
Warner, M.J., Bullister, J.L., Wisegarver, D.P., Gammon, R.H., Weiss, R.F., 1996. Basin-wide distributions of chlorofluorocarbons CFC-11 and CFC-12 in the North Pacific: 1985–1989. J. Geophys. Res. 101, 20525–20542.
Warner, M.J., Weiss, R.F., 1985. Solubilities of chlorofluorocarbons 11 and 12 in water and sea water. Deep-Sea Research 32 (12), 1485–1497.
Warner, M.J., Weiss, R.F., 1992. Chlorofluoromethanes in South Atlantic Antarctic intermediate water. Deep-Sea Res. 39, 2053–2075.
Warren, B.A., 1983. Why is no deep water formed in the North Pacific. J. Mar. Res. 41, 327–347.
Weiss, R.F., Bullister, J.L., Gammon, R.H., Warner, M.J., 1985. Atmospheric chlorofluoromethanes in the deep equatorial Atlantic. Nature 314, 608–610.

Weiss, R.F., Bullister, J.L., Warner, M.J., Van Woy, F.A., Salameh, P.K., 1990. Ajax expedition chlorofluorocarbon measurements, SIO reference 90-6, Scripps Institution of Oceanography, University of California, San Diego.

Williams, R.G., Spall, M.A., Marshall, J.C., 1995. Does Stommel's mixed layer "Demon" work? J. Phys. Oceanogr. 25, 3089–3102.

WOCE Data Products Committee, 2000. WOCE Global Data,Version 2.0. WOCE Report No. 171/00, WOCE International Program Office, Southampton, UK.

Yamanaka, Y., Tajika, E., 1996. The role of the vertical fluxes of particulate organic matter and calcite in the oceanic carbon cycle: studies using an ocean biogeochemical model. Global Biogeochem. Cycles 10, 361–382.

Zheng, M., De Bruyn, W.J., Saltzman, E.S., 1998. Measurements of the diffusion coefficients of CFC-11 and CFC-12 in pure water and sea water. J. Geophys. Res. 103, 1375–1379.

Zwally, H.J., Comiso, J., Parkinson, C., Campbell, W., Carsey, F., Gloerson, P., 1983. Antarctic Sea Ice, 1973–1976: Satellite passive microwave observations, 206 pp.